Canadian Science Publishing
NRC Research Press journals | Publishing Services

Canadian Geotechnical Journal
Revue canadienne de géotechnique

Load transfer platform behaviour in embankments supported on semi-rigid columns: implications of the ground reaction curve

Journal:	*Canadian Geotechnical Journal*
Manuscript ID	cgj-2016-0406.R1
Manuscript Type:	Article
Date Submitted by the Author:	07-Jan-2017
Complete List of Authors:	King, Daniel; Monash University, Civil Engineering Department; Golder Associates Pty Ltd, Bouazza, Abdelmalek; Monash University, Gniel, Joel; Golder Associates Pty Ltd, Rowe, Kerry; Queen's University, GeoEngineeering Centre at Queen's RMC Bui, Ha; Monash University, Civil Engineering
Keyword:	Arching, geosynthetics, load transfer platform, column supported embankment, field case study

Load transfer platform behaviour in embankments supported on semi-rigid columns: implications of the ground reaction curve

Authors:

Daniel J. King[1]

Abdelmalek Bouazza[2*]

Joel R. Gniel[3]

R. Kerry Rowe[4]

Ha H. Bui[5]

*Corresponding author

[1]PhD student, Department of Civil Engineering, 23 College Walk, Monash University, Melbourne, Vic. 3800, Australia. Email: daniel.king@monash.edu
Geotechnical Engineer, Golder Associates Pty. Ltd. Building 7, Botanicca Corporate Park, 570 – 588 Swan Street, Richmond, Vic. 3121, Australia. Email: dking@golder.com.au

[2] Professor, Department of Civil Engineering, 23 College Walk, Monash University, Melbourne, Vic. 3800, Australia. Email: malek.bouazza@monash.edu

[3] Associate, Principal Geotechnical Engineer, Golder Associates Pty. Ltd. Building 7, Botanicca Corporate Park, 570 – 588 Swan Street, Richmond, Vic. 3121, Australia. Email: jgniel@golder.com.au

[4] Professor and Canada Research Chair in Geotechnical and Geoenvironmental Engineering, GeoEngineering Centre at Queen's-RMC, Queen's University, Ellis Hall, Kingston, ON, Canada K7L 3N6. Email: kerry.rowe@queensu.ca

[5] Senior Lecturer, Department of Civil Engineering, 23 College Walk, Monash University, Melbourne, Vic. 3800, Australia. Email: ha.bui@monash.edu

Abstract:

Post-construction data from an instrumented geosynthetic reinforced column supported embankment (GRCSE) on drilled displacement columns in Melbourne, Australia, shows the time-dependent development of arching over the two-year monitoring period and a strong relationship between the development of arching stresses and sub-soil settlement. A ground reaction curve is adopted to describe the development of arching stresses and good agreement is found for the period observed thus far. Predictions of arching stresses and load transfer platform behaviour are presented for the remaining design life. Four phases of arching stress development (initial, maximum, load recovery and creep strain phase) are shown to describe the time-dependent, and sub-soil dependent, development of arching stresses that can be expected to occur in many field embankments. Of the four phases, the load recovery phase is the most important with respect to load transfer platform design as it predicts the breakdown of arching stresses in the long-term due to increasing sub-soil settlement. This has important implications in assessing the appropriate design stress for the geosynthetic reinforcement layers but also the deformation of the load transfer platform in the long term.

Keywords: Arching, geosynthetics, load transfer platform, column supported embankment, field case study

Introduction

Ground improvement using geosynthetic reinforcement and column supported embankments (GRCSEs) is an increasingly popular design solution to support embankments for road and rail applications. A significant quantity of research has been reported on this topic over the past two decades as documented in current literature (Han and Gabr 2002; Chen *et al.* 2008; Briançon and Simon 2011; Filz *et al.* 2012; van Eekelen *et al.* 2013; Rowe and Liu 2015; Liu and Rowe 2015). Emphasis of this research work particularly focussed on the description of the complex soil-structure-geosynthetic reinforcement interaction occurring in the load transfer platform (LTP) at the base of an embankment. The unreinforced concrete columns (refereed to subsequently as drilled displacement columns or simply columns) examined in this paper represent a semi-rigid ground improvement technique and are not designed subject to the same performance criteria as a pile. It is necessary to achieve sufficient penetration into a founding material in order for the "semi-rigid" column to achieve an appropriate (axial) stiffness. This approach is consistent with the nomenclature widely used in the North American literature (e.g., Wachman and Labuz 2008; Filz 2012). Owing to the increased use of GRCSE, national design methods have been developed in several countries such as Germany (EBGEO 2010), United Kingdom (BS8006-1 2010) and the Netherlands (CUR226 2010). However, the various design methods presented calculated arching stresses that differed considerably (Naughton and Kempton 2005; Lawson 2012) and, in addition, they differed from those measured in the field (Haring *et al.* 2008; van Eekelen *et al.* 2010; van Eekelen and Bezuijen 2012a). To gain a better understanding of the LTP behaviour and overall embankment performance a research project has been undertaken in Melbourne, Australia, where a recently constructed railway embankment has been extensively instrumented and monitored. The objective of this paper is to examine the localised LTP behaviour, including the development of arching stresses and interaction with geosynthetic reinforcement observed in the embankment. The global scale embankment behaviour, ground improvement and column installation effects are examined in a separate paper.

Background

The LTP design generally follows a two-step process: Step 1 - assessment of arching and calculation of load acting on semi-rigid columns (part A load) and load acting in the area between columns (parts B + C load); Step 2 - separation of load in parts B + C, this step calculates the tensile load taken by the geosynthetic reinforcement (part B) as well as the load supported by the subsoil (part C) in the area between columns. A significant number of models exist for calculating the arching stresses in Step 1. Van Eekelen *et al.* (2013) categorised about 20 models as either rigid, limit equilibrium, frictional, mechanical or empirical models while McGuire and Filz (2008) presented a parametric analysis of 10 of these models. However, many of these models were shown to provide predictions of arching stresses that differed considerably for various embankment geometries and material properties (Ellis and Aslam 2009b and Lawson 2012) and more importantly, these models have been shown to differ from field behaviour. As a result, additional models have been developed in recent years such as the concentric arches (CA) model (van Eekelen *et al.* 2013) based on extensive laboratory testing (van Eekelen *et al.* 2012b, 2012c) and validated against several field case studies (van Eekelen *et al.* 2015) as well as a simplified method by Zhuang *et al.* (2014). Of the large number of models available, the limit-equilibrium models have received the most attention. The model of Hewlett and Randolph (1988) was adopted in the French ASIRI guideline and suggested as an alternative in BS8006-1 (2010), the model of Zaeske (2001) was incorporated into EBGEO (2010) and CUR226 (2010) and more recently the CA model was proposed for the revised Dutch standard (CUR226 2015). These methods calculate the stress acting on the area between columns based on geometric parameters (column spacing s, column head width a, and embankment height h) and LTP material parameters (effective friction angle ϕ'). The result is a value of stress acting on the geosynthetic reinforcement layer/sub-soil (Part B +C) which is independent of sub-soil consolidation and time. However, the CA model does describe qualitatively increasing arching stresses due to sub-soil consolidation but the quantitative output of the model is the same as other limit-equilibrium models. This two-step design approach has the effect of de-coupling the arching stress-displacement relationship as the

displacement calculated in the second step is based on a constant value of arching stress from the first step (independent of displacement).

The relationship between arching stresses and displacement is well documented in trapdoor tests as far back as Terzaghi (1936) and extended further by Iglesia *et al.* (1999, 2013) who developed the so-called Ground Reaction Curve (GRC) to describe the relationship between arching stresses and displacement. The GRC is calculated based on simple geometric and material properties, similar to limit equilibrium models, and plotted as a function of relative displacement (displacement/trapdoor width) which is typically expressed as a percentage. The fundamental mechanisms governing the development of arching as assessed through trapdoor tests and described by the GRC concept has been referred to by only a handful of researchers (Aslam and Ellis 2008; Ellis and Aslam 2009a, 2009b, Zhuang *et al.* 2012; Iglesia and Einstein 2015) in the context of column-supported embankments, despite the similarities between the two problems. However, a number of researchers have observed in laboratory and field scale studies variations in arching stresses attributed to sub-soil settlement. Chen *et al.* (2008) described a laboratory scale model with 2D bearing elements and sub-soil consolidation controlled by a water bag. Based on stress-displacement plots of measured arching stresses and the stress concentration ratio, it was noted that "*soil arching is strongly dependent on pile-subsoil relative displacement*" and went further to describe, using terminology similar to that which describes the GRC, a critical relative displacement where arching was most efficient. Similar behaviour was observed by van Eekelen *et al.* (2012b) through multiple loading-consolidation steps, with load component A observed to increase during consolidation steps. However, in these laboratory scale models, rather than slow controlled sub-soil consolidation like that which occurs in the field, the subsoil support was removed quickly and the arching stress-displacement relationship was simply described as "increasing" during the consolidation stage.

Of the limited number of full-scale instrumented embankments described in the literature (Haring et *al.* 2008, Wachman and Labuz 2008, van Eekelen *et al.* 2010, van Eekelen *et al.* 2012), one feature is common throughout; the time-dependent development of arching stresses (measured through earth pressure cell (EPC) data) which in many cases continued well into the post-construction phase. This time-dependency is a manifestation of the time-dependent consolidation of the soft soil

underlying the embankment (i.e., the time dependent loss of sub-soil support). This time-dependent behaviour observed in field studies cannot be described with the existing arching models typically used for column-supported embankment design. Laboratory testing used to develop the GRC showed that maximum arching occurred at relatively small trapdoor displacements. However, at larger displacements, arching began to break down (Iglesia 1991; see also Terzaghi 1936; Ladanyi and Hoyaux 1969; and Evans 1983). In the context of full scale column-supported embankments, this displacement range for which arching breaks down is expected to occur within the typical displacement range of the geosynthetic reinforcement. The increase of arching stresses acting on the geosynthetic reinforcement at larger sub-soil displacements (or larger deflection of the reinforcement) has important implications for GRCSE design.

This paper examines the design and construction of a GRCSE constructed as a widened embankment requiring a split-level LTP. To the authors' knowledge, an embankment design of this type has not been documented in the literature previously. The interaction between the two LTP levels is also described. Based on this, the primary objective of this paper is to show, based on over 2 years of monitoring data, that the development of arching stresses at the base of the embankment can be described using the concept of the Ground Reaction Curve (GRC) proposed by Iglesia *et al.* (1999, 2013); and hence provide new insight into the behaviour of the LTP and interaction with the geosynthetic reinforcement. The GRC is compared with the field data gathered thus far and then used to predict the long term LTP behaviour over the remaining design life of the embankment. The relationship between arching stresses and subsoil settlements is shown.

Given the considerable amount of time needed to observe the full development of arching stresses, field scale examples are extremely limited. The embankments described by Wachman and Labuz (2008) and van Eekelen et al (2010) presented EPC data that was, to the authors' knowledge, the only full scale embankments which demonstated the development of maximum arching and the breakdown of arching over the long term. The EPC stress data from these embankments showed near identical characteristics of the GRC (i.e. initial, maximum and load recovery phases of arching). The implications that these developments pose for the design of GRCSE are discussed. It is also shown that the concept of varying arching stresses as a function of sub-soil settlement provides some insight

as to why various design methods frequently provide results that differ with measured in-situ arching stresses; the displacement range at which stresses are compared are not consistent. Furthermore, this provides insight as to why measured geosynthetic reinforcement tensile loads and strains, which are directly related to the development of arching stresses and sub-soil settlement, also differ from those predicted based on the current design methods.

The intention of this paper is not to validate the GRC method as the preferred arching model but rather to highlight how the phases of arching development described by the GRC method (initial arching, maximum arching and the load recovery phase) affect the behaviour of the LTP. In addition, it is the aim of this paper to highlight that an arching model must incorporate sub-soil settlement as a governing parameter to describe accurately the development of arching.

Field case study

The Regional Rail Link project in Victoria, Australia, saw the construction of a new rail link between regional Victoria and the Melbourne CBD in addition to significant upgrades to existing rail infrastructure. At the time, the project was the largest public infrastructure project in Australia. A 4.5 km length of the proposed rail alignment located in the inner west of Melbourne was delivered by the Regional Rail Link – City to Maribyrnong River (RRLCMR) Alliance. This particular section of the overall alignment posed numerous challenges from a geotechnical perspective. This was largely due to approximately 80% of the alignment being underlain by a local soft soil known as Coode Island Silt. To meet rail performance criteria and minimise construction time, four basal reinforced column-supported embankments were constructed along the alignment by the RRLCMR Alliance (Fig. 1). These works comprised the installation of over 1900 drilled displacement columns and a combined embankment length of over 760 m.

One of the Maribyrnong River embankments was described separately by Gniel and Haberfield (2015). The North Dynon embankment was selected for instrumentation and monitoring as part of the ongoing research work. It is the subject of this paper.

Subsurface conditions

The subsurface conditions have been assessed based on a large amount of geotechnical investigation information available from the project (between 2009 and 2013), historic works and additional laboratory testing undertaken for the purpose of this research project. The general sub-surface conditions in the vicinity of the embankment were identified based on 16 boreholes and 18 Cone Penetration Tests (CPTs). CPT28 to CTP31 and CPT11 were performed as part of detailed design and were the primary source of information for the ground improvement works. An additional borehole BH41 was drilled for research purposes immediately adjacent to CPT31. The geological setting in this area comprises Quaternary aged Yarra Delta sediments (Coode Island Silt and Fishermens Bend Silt at this site) which have infilled a Tertiary aged paleo valley associated with the ancestral course of the Moonee Ponds Creek. The present day Moonee Ponds Creek is situated immediately to the east of the embankment. The Yarra Delta sediments are encountered throughout the Melbourne city area and their geological and engineering properties are well described by Neilson (1992) and Ervin (1992), respectively. Within the Yarra Delta group of sediments, the near-surface Coode Island Silt, is of particular importance owing to its wide spatial distribution, low undrained shear strength (s_u typically increases from about 15 kPa to 40 kPa at depth) and its considerable thickness of up to 25 m in parts. Despite their geological names, the Coode Island Silt encountered is almost exclusively a silty clay while the Fishermens Bend Silt is an over-consolidated clay to sandy clay. A detailed description of the sub-surface conditions, laboratory testing and assessment of in-situ testing of the Coode Island Silt data was presented in King *et al.* (2016). Laboratory testing performed included: Atterberg limits, particle size distribution (PSD), 15 automated oedometer tests and 8 manual oedometer tests with an extended (one-week) creep incremental load stage. Selected results from King *et al.* (2016) are presented below, with a particular emphasis on the settlement characteristics of the Coode Island Silt, which are relevant for the settlement analysis presented later in this paper.

A geological long section of the ground improvement zone (chainage 2450 m to 2515 m) where the instrumented sections of the embankment are located is presented in Fig. 2a. The Moonee Ponds creek is at approximately chainage 2420 m to 2440 m and CPT11 is at chainage 2445 m. The

thickness of the Coode Island Silt can be seen to increase considerably towards the eastern end of the embankment adjacent to the creek. As-built records of the installed columns have been used here to refine the geological long section. The corrected cone tip resistance (q_t) profiles of CPT29, CPT30 and CPT11 are presented in Fig. 2 a, b, c and d, respectively. In addition, the soil behaviour type zone is shown, this is calculated based on the CPTu material index (I_c) (equation [1] after Jefferies and Been 2006) and the values presented in Fig. 2.

[1] $$I_c = \sqrt{\{3 - \log(Q_t[1 - B_q] + 1\}^2 + \{1.5 + 1.3\log(F_r)\}^2}$$

The three normalised CPTu parameters are calculated as follows: normalised cone tip resistance $Q_t = (q_t - \sigma_{v0})/\sigma'_{v0}$, normalised friction ratio $F_r = 100\ \% \times f_s/(q_t - \sigma_{v0})$ and normalised porewater pressure $B_q = (u_2 - u_0)/(q_t - \sigma_{v0})$. Where f_s is sleeve friction, u_2 pore water pressure, σ_{v0} total vertical stress, σ'_{v0} effective vertical stress and u_0 is the hydrostatic porewater pressure. The undrained shear strength profile (s_u) for various CPTs has been calculated as $s_u = (q_c - \sigma_{v0})/N_k$ (Fig. 2e). CPT11 has been calibrated against (corrected) in-situ shear vane tests performed in the immediate vicinity of this test location. A cone factor (N_k) of 15 was found to provide an excellent fit with a linear trendline through the shear vane data (Fig. 2e); this compares well with similar locally calibrated CPT profiles reported by Ervin (1992) and Srithar (2010).

Based on the pre-consolidation stress (σ'_p) profile obtained from the laboratory investigation it was found that the expression $\sigma'_p = k(q_t - \sigma_{v0})$, with a value of $k = 0.3$ by Lunne *et al.* (1997), provided an excellent correlation between the cone resistance (CPT31 adjacent to BH41) and the pre-consolidation stress (King *et al.* 2016). Values of secant compression index (C'_c) calculated from the automated oedometer test data are also reported by King *et al.* (2016). Additional parameters relating to the fill unit, Coode Island Silt and Fishermens Bend Silt are summarised in Table 1. The water level in the Moonee Ponds Creek is tidally influenced and generally fluctuates between relative level (R.L.) 0.2 m and R.L. 0.9 m. The groundwater is encountered beneath the embankment at R.L. 0.6 m based on historic data and data from an installed piezometer.

Basal reinforced column-supported embankment design

The widened North Dynon embankment comprises four design zones over a length of about 180 m. The field case study focuses on the 60 m length of embankment at the eastern end of the embankment where ground improvement was required. The other three design zones had more favourable ground conditions and as a result did not require ground improvement. It was necessary to design and construct a split-level LTP comprising lower and upper levels to minimise the potential for settlement beneath the existing rail embankment. To minimise the footprint of the embankment, a near-vertical gabion wall was constructed in favour of a batter slope. The embankment design is summarised below:

- Drilled displacement columns are 450 mm diameter, installed with a minimum 2 m-long socket into the underlying stiff to very stiff clay Fishermens Bend Silt and were designed for a working load of 700 kN. Each displacement column had an enlarged 1 m square head constructed at the ground surface by excavating 1 m square by approximately 600 mm deep and backfilling with concrete, typically, while the concrete of the column was still wet.
- Drilled displacement columns were typically spaced on a square 2.5 m by 2.5 m grid, or 2.0 m by 2.0 m near the eastern end of the embankment. However, these spacings varied in places due to geometric constraints.
- The LTP comprised a 650 mm thick layer of 75 mm minus granodiorite rockfill with two layers of geogrid reinforcement. The particle size distribution curve indicated values of coefficient of curvature (C_c) of 2.41, uniformity coefficient (C_u) of 150 and equivalent particle diameters at 10%, 30 % and 60% passing (D_{10} = 0.1 mm, D_{30} = 1.9 mm and D_{60}= 15.0 mm). Typical lower and upper particle size distribution curves are presented in the Supplementary Material Section[1]. Since the 75 mm minus rockfill was too large for the shear box used, a scaling technique based on Lowe (1964) was used. Using this parallel gradation technique, a scaling factor of 2.8 was obtained and used to estimate the shear strength properties of the rockfill. Thus the direct shear tests were conducted on material with a similar grain size distribution but all grain sizes reduced by a factor of 2.8 (see Supplementary Material Figure S3). Tests were performed using the Monash

University's Constant Normal Stiffness (CNS) direct shear apparatus (Haberfield and Szymakowski 2003) which has a shear box measuring 600 mm x 200 mm (135 mm high). Peak secant (effective) friction angles of 51°, 49° and 44° were obtained at vertical stresses of 50 kPa, 100 kPa and 200 kPa respectively, as described in more detail in the Supplementary Material (Section 2)[1].The measured values of friction angle are consistent with the curvi-linear nature of the failure envelope for rockfill material at low confining stresses.

- The LTP geosynthetic reinforcement installed was ACEGrid® GG200 uniaxial polyester geogrid and comprised a transverse layer placed 100 mm above the column heads and a longitudinal layer placed 100 mm above the transverse layer. The geogrid material properties as reported by the manufacturer are presented in Table 2. Additional laboratory testing of the geogrid was undertaken as part of the strain gauge calibration presented later in this paper.
- The height of gabion wall varied from 3 m to 6.5 m in height at the eastern end.
- The embankment fill material is a silty sandy gravel (GM), comprising 40 to 55 % gravel, approximately 30 % sand and the remaining portion comprising low plasticity inorganic fines. The fill material was placed in loose layers not exceeding 300 mm and compacted to 95 % standard Proctor compaction; the upper 1 m of the embankment was compacted to 98 % standard Proctor compaction. The results of 12 compaction assessments using the nuclear gauge method (AS 2007) indicated an average field dry and wet density (average water content w of 13.3 %) of 19.2 kN/m^3 and 21.7 kN/m^3, respectively.

The two areas of the North Dynon embankment where the instrumentation was installed (Area #1 and Area #2) are shown in plan view in Fig. 3. An embankment cross section of Area #2 is presented in Fig. 4 and an additional cross section of Area #1 is presented with the Supplementary Material (Fig. S1).[1]

[1] Supplementary data are available with the article through the journal Web site at (**link**)

Instrumentation

General

A detailed layout plan of instrumented Area #2 is shown in Fig. 5 and the layout plan for Area #1 is shown in the Supplementary Material Section (Fig. S4)[1]. The instrumentation plans should be read in conjunction with the embankment plan view (Fig. 3) and cross-section (Fig. 4). The installed instrumentation comprised earth pressure cells (EPCs), strain gauges, vertical inclinometers, tiltmeters, piezometers and horizontal inclinometers. The installed EPCs and strain gauges are described below. The other instrumentation is the subject of a separate paper and is not presented here. For the instrumentation data presented in this paper, time zero is defined as 3 May 2013 8:00 am; the first readings from Area #2 were taken at this time. The first automated reading from the data acquisition hardware was taken on day 96 (7 August 2013 at 12:50pm), prior to this date readings were taken manually. Details of the data acquisition hardware are presented in King (2017).

Earth pressure cells

To measure the load distribution associated with arching, three EPCs were installed within the LTP in both instrumented areas. The Geokon model 4800 circular EPCs installed have a 230 mm diameter and are 6 mm thick (aspect ratio of 38). The EPCs were numbered based on their installation order; EPC 1 was located 100 mm above column D15, EPC2 and EPC3 were both located at the centre of the grid of four columns. EPC2 was 150 mm below the base of LTP in the sub-soil and EPC3 was 550 mm above the column heads in the LTP material (100 mm below the top surface of the LTP). The EPCs installed in Area #1 were located in a similar manner (i.e., EPC4 was similar to EPC1, EPC5 to EPC2 etc.). However, EPC6 was located 750 mm above the top of the column head in the embankment fill material (100 mm above the top surface of the LTP). All EPCs were installed in a sand pocket measuring approximately 0.5 m by 0.5 m and 0.2 m high.

Strain gauges

Strain gauges (Vishay Micro-Measurements® (VMM) type CEA-06-250UN-350) were installed in pairs on the longitudinal and transverse layers of the geogrid on the machine direction ribs to ensure the repeatability of the results. For Area #2, four pairs of gauges were installed on the longitudinal

geogrid, six pairs on the transverse geogrid and two dummy gauges (22 gauges total) were installed (Fig. 5a). To calibrate against thermally induced strain, dummy gauges on 5 cm pieces of geogrid separate from the reinforcement layers were installed in the rockfill. The gauges were installed (see Supplementary Material for further details)[1] in accordance with the detailed procedure described by Oglesby *et al.* (1992) for bonding strain gauges to woven polyester (PET) geogrids and general recommendations in the VMM literature.

Strain gauge calibration was performed in order to establish the relationship between localised strain (strain gauge reading) and global geogrid strain. These tests were performed in accordance with ASTM D6637-11 with global geogrid strain measured using an Instron – Non-contacting Standard Axial Video Extensometer 2. This approach provided a high resolution, non-contact measure of global geogrid strain and removed errors associated with clamp slippage typically encountered with the testing of high tensile strength geosynthetic materials (Shinoda and Bathurst 2004). The calibration factor obtained is dependent on a range of factors; the predominant factors include: geosynthetic material type, ultimate tensile strength and strain gauge application procedure. This has been shown by Bathurst et al (2002), who summarised the calibration factors obtained from 12 studies; a range of 1.0 to 2.0 for mostly low strength geogrids was shown. These calibration factors indicate that the application of glue/epoxy creates a localised stiff spot (i.e. strain gauge reading is less than global strain). By contrast, the application of the strain gauge to the high-strength (200 kN/m) PET geogrid used in the present study creates a localised "soft" spot; in the present study a calibration factor of 0.82 was obtained. The localised gauge reading is therefore greater than the registered global strain. Laboratory testing by Oglesby *et al.* (1992) using this gauge application technique on similar high-strength (T_{ult} = 133 kN/m) woven PET geogrid observed similarly consistent behaviour although with a slightly lower calibration factor. Further details of the laboratory testing are provided in the Supplementary Material Section[1].

[1] Supplementary data are available with the article through the journal Web site at (**link**)

Embankment construction timeline

The construction sequence for the North Dynon embankment is outlined in Table 3 and the embankment height measured at Area #2 is shown in Fig. 6. The embankment height is defined relative to the base of the LTP (R.L. +2.0 m). The split-level LTP design meant that lower and upper level ground improvement works were undertaken in stages. Due to the need to relocate a number of underground assets near the eastern end of the embankment, construction was not uniform along the length of the embankment. As a result, the western end (Area #2) progressed well ahead of the eastern end (Area #1) during construction. The ground improvement works for the lower LTP (Stage 1 and 2) and upper LTP (Stage 3a and 3b) were separated into additional phases for this reason. This inadvertently benefited the instrumentation program as it allowed additional time between the installations. The embankment construction involved a total of seven embankment lifts plus track formation. The lower portion of the embankment required the completion of Stage 1 and 2 works, the partial construction of the gabion wall and the construction of the lower LTP and embankment lifts 1 and 2. Following this, the Stage 3a and 3b upper level works were completed followed by the remainder of the gabion wall and embankment lifts 3 to 7.

Field case study results

Preliminary field observations have been described previously by King *et al.* (2014) based on construction phase data and a limited amount of post-construction data. This paper expands on the initial observations described in King *et al.* (2014) and presents an analysis of the arching stress development which was not previously possible based on the limited data available at the time. Temperature sensors in the earth pressure cells have been used to assess long-term temperature variation in the instrumented areas. In Area #2 the long term seasonal variation can be approximated by a sinusoidal function with a mean temperature of 16.9 °C and a seasonal fluctuation of ±2.0 °C. The effects of both daily and seasonal temperature variation on the strain gauge readings are discussed

in the Supplementary Material.[1] However, despite the small values of strain observed to date, these temperature effects are still relatively small by comparison.

Earth pressure cell data - Area #2

The EPC data for Area #2 is shown in Fig. 7 along with the embankment height. Only the first 400 days are plotted to show the development of the arching stresses more clearly. The measured stresses match closely with the overburden stress during the first 20 days (LTP placement; Fig. 7). Partial arching is observed as an increase in EPC1 and a reduction in EPC2 after embankment lift #1 (days 34 to 46) where the embankment height increased from 0.65 m to 1.90 m. By day 80 the arching behaviour is well established. However, there are two events which had a considerable effect on the measured stresses and were related to where columns were installed as part of the Stage 3a and 3b works. The measured data shows that the arching collapses on day 136 and again on day 137 as a result of the installation of several columns near the already constructed lower LTP. On days 136, 137 and 138 the arching stresses are observed to collapse and both EPC1 and EPC2 return to an overburden stress condition (57 kPa).

The location of the upper level columns relative to the lower level LTP and instrumentation area was shown in Fig. 4. Fig. 8 shows that the variation in arching stresses between days 130 and 139 matches with the installation of the nearby columns. Note that the arching lost due to column installation was re-established shortly after column installation, as is evident after working days 133, 136 and 137 and after the Stage 3a works. A power outage caused loss of data between days 139 and 146.

Strain gauge data - Area #2

At this point in time it is difficult to undertake detailed analysis of the strain gauge data as the sub-soil settlement is estimated to be quite small (discussed later in the paper), i.e., the geogrid has only been partially mobilised at this time. The transverse strain gauges (Fig. 9a) show a variable response over the small strain range presented; this is primarily due to the small subsoil settlement over the period being examined. The initial strain in the geogrid layers at placement (in some areas the geogrid was more taut than in others areas) is also likely a contributory factor. This was the first of four layers of

[1] Supplementary data are available with the article through the journal Web site at (**link**)

geogrid installed and some difficulties were encountered with transportation and installation that were rectified with the installation of the next three layers of geogrid. A number of these gauges failed, others showed quite an erratic response, only a small number of gauges indicated long-term strains that are consistent with the expected membrane action. A number of longitudinal strain gauges showed erratic results, however, four of these gauges indicated increasing strain between days 150 to 180 (embankment lifts 3 to 7) and gradual increase post-construction. Tensile strain of about 0.10 % to 0.15 % was observed to have developed in the geogrid layer. These small values of tensile strain observed are consistent with the geogrid having only a minor role at this point in time. Further discussion of the strain gauge data is presented in the Supplementary Materials Section[1]. As the geogrid is fully mobilised in the future, further analysis of the strain gauge data will be possible. These values of strain data observed to date are compared with predictions of the sub-soil settlement in later sections and good agreement is found.

Area #1 data

The development of arching stresses in Area #1 shows similar behaviour with a reduction in vertical stress in the area between columns. However, it is difficult to assess the arching stress development further due to the influence of the upper level LTP which is located immediately adjacent to the Area #1. For this reason, the earth pressure cell data and strain gauge data from Area #1 are provided for completeness in the Supplementary Material Section.[1] The analysis in the following sections focuses on the Area #2 data.

Analysis of results

The following sections examine the development of the arching stresses with emphasis on the relationship between the sub-soil settlement and the arching stresses. This analysis involves four steps and provides the basis by which a designer can evaluate the development of arching stresses. The output of this analysis is compared with the data observed to date and predicted arching stresses for the remaining design life of the embankment are presented.

[1] Supplementary data are available with the article through the journal Web site at (**link**)

1. **Overburden stress** – knowledge of the overburden stress is required, this is assessed using a 2D plain strain finite element model.
2. **Ground Reaction Curve** – a predicted GRC curve describing the relationship between arching stresses and sub-soil settlement is developed based on the procedure described by Iglesia *et al.* (1999). This is compared with the measured arching stresses.
3. **Settlement analysis** - as no direct measurement of the sub-soil settlement is available the sub-soil settlement is assessed through a detailed settlement analysis and compared with the GRC.
4. **Strain gauge results** – the development of tensile strain in the geogrid layers due to the downward sagging of the geogrid is used to back-calculate geogrid deflection and also compared with the GRC.

Overburden stress

The stress reduction ratio is a parameter typically used to quantify the degree of arching. It is defined as $\sigma'_v/\ \sigma'_{v0}$ where σ'_v is the stress acting in the area between columns and σ'_{v0} the initial effective overburden stress. The overburden stress can be assessed by a simple one-dimensional calculation at the location of EPC2; a value of 70.4kPa is obtained. To account for geometry of the embankment and the presence of the gabion wall (Fig. 4), a 2D plain strain finite element analysis was performed to more accurately assess σ'_{v0}. At the location of Area #2 (3.6 m of overburden material), σ'_{v0} was assessed to be 74 kPa (details of the analysis are presented in the Supplementary Material section)[1].

The stress acting on the area between columns measured by EPC2 is used to assess the stress reduction ratio. The assumption is made that the load taken by the geogrid layer is negligible, this is a valid assumption for the initial period of arching assessed and it will be shown that the strain gauge readings validate this assumption. The EPC data presented previously is re-produced in Fig. 10 with the stress reduction ratio values shown for two periods where arching stresses develop; between Stages 3a and 3b works and post Stage 3b works. After Stage 3a works, the stress reduction ratio curve reduces from an initial value of 1.0 to 0.58 before the arching collapses due to the Stage 3b

[1] Supplementary data are available with the article through the journal Web site at (**link**)

works. The arching develops again over a period of nearly 1.5 years as the stress reduction ratio reduces to 0.08. In the following section, it is shown that these measured arching stresses can be calculated using the GRC (Iglesia *et al.* 1999, 2013).

Ground Reaction Curve (GRC)

The GRC describes the relationship between the stress reduction ratio and relative displacement (defined as trapdoor displacement / trapdoor width × 100%), or in the context of a GRCSE, a relationship between the development of arching stresses and sub-soil settlement. This was first described by Iglesia *et al.* (1999) primarily for tunnelling applications based on centrifuge modelling and was presented in further detail to describe more generally the development of arching in a soil mass (Iglesia *et al.* 2011, 2013). Here, the GRC is calculated based on two geometric parameters (height of soil mass above trapdoor H and trapdoor width B), material parameters of the granular material above the trapdoor (friction angle ϕ and mean particle size D_{50}) and the equations presented in Iglesia *et al.* (1999, 2013). An example of a GRC is shown in Fig. 11, the five characteristic features shown include: 1) initial arching phase, 2) minimum normalised loading (maximum arching), 3) break point and secant modulus of arching, 4) terminal phase and 5) load recovery index. Since this model was developed based on tests on dry granular material, the total stress is equal to effective stress. The phases of soil arching shown in Fig. 11 (initial, maximum, load recovery and terminal) have also been shown in laboratory testing by Terzaghi (1936), Ladanyi and Hoyaux (1969) and Evans (1983) amongst others.

In the authors opinion, the GRC is well supported by decades of laboratory research which has investigated the soil arching phenomena through the use of the trapdoor test. This research includes the work of Terzaghi (1936, 1942), Ladanyi and Hoyaux (1969), Vardoulakis et al. (1981), Evans (1983), Stone (1988), Ono and Yamada (1993), Dewoolkar et al. (2007) and Costa et al. (2009) amongst others. These studies have developed a relatively consistent interpretation of the arching development which is characterized by the simultaneous development of both internal and external shear bands during an active (downward moving) trapdoor test. Stone (1992) and others (Evans, 1983 and Santichaianant, 2002) have shown that internal shear bands propagate from the corner of the

trapdoor at an angle, inclined from the vertical, and equal to the dilatancy angle (a variable of relative density and confining stress) at that point in time. The curvature of the internal shear bands reflects variation in the dilatancy angle as the overburden stress reduces along the length of the shear band. It is the first internal shear band which broadly characterises the development of maximum arching, and the final external shear band which characterises the terminal phase of arching. Intermittent with these phases are additional internal failure surfaces which develop during the load recovery phase and are associated with the breakdown of the arching mechanism. Given the typical range of sub-soil settlement/geogrid deflection in a GRCSE, it is the phases of maximum arching and load recovery (and not the terminal phase) which are of interest to GRCSE. Iglesia *et al.* (1999, 2013) characterised the load recovery phase of arching as successive triangular failure surfaces (which occur with additional trapdoor displacement), with each failure surfaces forming an apex that is closer to the ground surface (i.e. internal failure surfaces moving upwards with additional trapdoor displacement).

In recent years, advanced imagining techniques have enabled improved visualisation of deformation patterns and the localised strain development (shear banding) which characterises the internal and external failure surfaces. Stone (1992) used digitized photographic and radiographic records to relate shear band development to dilatancy angle in active trapdoor tests, and recently, Jacobsz (2016) used Particle Image Velocimetry (PIV) techniques to provide high resolution imagery of shear band development over a large displacement range in the trapdoor tests.

Load transfer platform behaviour

To apply the GRC concept to the field case study it is necessary to convert the 3D embankment geometry to an equivalent 2D axisymmetric unit cell with parameters h (height of overburden material) and equivalent axisymmetric clear spacing (b). The embankment geometry at Area #2 is shown in Fig. 12 and has been converted to an equivalent axisymmmetric unit cell based on an equal area concept. A value of b = 1.42 m is calculated and a value of h = 3.9 m is adopted as this gives a value of overburden stress σ'_{v0} equal to 74 kPa (assessed in the preceding section). A friction angle (ϕ) of 50° and a mean grain size (D_{50}) of 9.7 mm are selected for the rockfill material based on the

laboratory data presented in this paper. The predicted GRC (based on Fig. 12) has been calculated based on the equations presented Iglesia *et al.* (1999, 2013) and is shown in Fig. 13. The stress reduction ratio values can be converted to a stress value by multiplying by the overburden pressure (σ'_{v0} = 74 kPa). Iglesia *et al.* (2013) noted that the intersection of the flat bottom portion of the GRC (zone of minimum loading) and the load recovery index line typically occurred between a relative displacement range of 3 % and 5 %. Thus in this paper, it was assumed to occur at a relative displacement of 4 %.

Based on the observed ground pressure at EPC2 (Fig. 10), the stress reduction ratio reduced from 1.0 to about 0.6 between Stage 3a and 3b works (day 68 to 131). Using the GRC, which establishes a relationship between arching stress development and sub-soil settlement, the phase of arching development and an estimate of sub-soil settlement can be assessed based on the observed EPC data. The variation in stress reduction ratio between Stage 3a and 3b, and the predicted GRC (Fig. 13), suggests that this arching stress development is consistent with an initial arching phase. In the 500 day period after Stage 3b works (Fig. 14), however, the development of maximum arching is evident and during this period the characteristics of the GRC match very well with the measured data. The measured data exhibits a flat bottom portion which matches well with the predicted minimum value of stress reduction ratio of 0.11. In addition, a localised point of maximum curvature, a characteristic of the GRC (breakpoint), is observed in the measured data at day 397, stress reduction ratio = 0.19. The linear line extending from the origin to the break point is termed the secant modulus and has a gradient of 63 in Fig. 11. The gradient of initial arching is 125 in Fig. 11 and is calculated in Fig. 14 based on the location of the observed breakpoint. This (theoretical) initial modulus of arching shown in Fig. 14 matches well with the inferred data (extrapolated 5th order polynomial) through the period of data loss. To assess the development of the arching stresses in further detail using the GRC, it is necessary to convert the arching stress *versus* time data (Fig. 10) to an arching stress *versus* sub-soil settlement plot by establishing a relationship between time and sub-soil settlement. This is done by fitting the measured stress reduction ratio curve in Fig. 14 to the predicted GRC in Fig. 13 by matching the characteristic features; breakpoint, flat bottom portion and initial straight line arching

514 phase. The result is the relative displacement axis shown in Fig. 14 (upper horizontal axis) which
515 establishes a relationship between days elapsed and sub-soil settlement. From these relative
516 displacement values, the magnitude of sub-soil settlement can be calculated by multiplying by *b* (i.e.
517 1.42m). The back-calculated sub-soil settlement where maximum arching (relative displacement =
518 2 %) is inferred to commence is calculated to be about 28 mm at day 537 (Fig. 14).

519 ***Comparison with settlement analysis***

520 The settlement analysis for Area #2 was performed based on the stress acting on the sub-soil
521 measured by EPC2 from day 137 onwards (Fig. 7). The Coode Island Silt was sub-divided into 3 sub-
522 layers with the parameters adopted for the settlement analysis (Table 4) based on the laboratory tests
523 described in King et al. (2016). The sub-surface materials at Area #2 were presented in the geological
524 long section (Fig. 2). The results of the settlement analysis are presented in Fig. 15. The settlement
525 analysis shown does not include secondary compression. The time-rate of settlement was assessed
526 using the time-U(%) relationship described by Srithar (2010) which was back-calculated from field
527 scale settlement data from Coode Island Silt sites (c_v = 2 m^2/year and H = 2.3 m). It is noted that this
528 settlement analysis is highly sensitive to the time rate of settlement parameters c_v (coefficient of
529 consolidation) and H (maximum drainage length). The results of a second analysis with H = 4 m is
530 shown in Fig. 15 to highlight this point. The difficulties in assessing accurately the presence of minor
531 sand lenses (i.e. representative values of c_v and H) in the Coode Island Silt is discussed by Srithar
532 (2010) and King et al. (2016). The implications this has on the settlement analysis presented is
533 discussed further in the Supplementary Materials section[1].

534 ***Comparison with strain gauge results***

535 Based on the strain gauge results presented in Fig. 9 the deflection of the geogrid layer can be
536 estimated using the simplified expression of Giroud (1995) for an assumed parabolic sagging geogrid
537 spanning a clear spacing ($s - a$):

$$[2] \qquad \text{Maximum sag} = (s - a)\sqrt{\frac{3\varepsilon}{8}}$$

[1] Supplementary data are available with the article through the journal Web site at (**link**).

For this case, the geogrid strip between columns D15 and D14 (Fig. 5) in Area #2 is considered, $s - a$ = 1.5 m. Based on the average strain (ε) of gauges 5N, 5S and 6N, the deflection is calculated using Equation [2] and presented in Fig. 15. Maximum geosynthetic sag can also be assessed using the design charts by Zaeske (2001) and presented in EBGEO (2010). Based on a maximum strain ε_k of 0.1 %, the $\Delta f/L_W$ value is 0.21 where Δf is the deflection of the geogrid layer and L_W the clear spacing (1.5 m). A maximum deflection of 32 mm is obtained from this method. Although both of these calculations ignore the localisation of strain in the geogrid layer as well as the 3D nature of the membrane deflection, the estimated deflection is generally consistent with the settlement analysis and the back-calculated settlement from the GRC.

Long term behaviour

From the settlement data presented in Fig. 15 there is reasonable agreement between the three predictions of sub-soil settlement (strain gauge, settlement analysis and back-calculated from arching stress development using the GRC) over the 500 day post-construction period shown. However, it is clear that the assumed linear relationship between back-calculated settlement (from the GRC) and time is incorrect (bottom and top horizontal axes in Fig 14.) As the applied stress acting on the Coode Island Silt reduces, and settlement transitions from settlement predominately due to normal consolidation, then consolidation in the re-compression range and finally creep compression. As a result, the relationship between sub-soil settlement and time is non-linear (this is discussed further in the Supplementary Materials Section[1]). At this time, the measured EPC data has shown arching stress development up to maximum arching; it is difficult to assess the non-linear relationship between sub-soil settlement and time without further EPC data to define fully the GRC. For this reason, we have assumed a linear relationship, which despite the limitations of this assumption, shows reasonable agreement with the settlement analysis and strain gauge assessment of sub-soil settlement (Fig. 15).

The most important feature of the GRC with respect to the LTP behaviour is the transition from maximum arching to a load recovery phase associated with the breakdown of the arching mechanism. This has important implication for the design of the geogrid layer as this suggests the

[1] Supplementary data are available with the article through the journal Web site at (**link**).

stress acting on the geogrid layer will begin to increase at some time in the future, and will continue to increase to the ultimate value of stress reduction ratio, unless displacement in the area between columns is arrested by the geogrid layer. The development of arching described by the GRC invokes the following question: At what relative displacement will loss of subsoil support occur? Without a direct measurement of the sub-soil settlement, accurately assessing when the loss of subsoil support will occur is difficult in this particular case due to variability of the sub-surface conditions caused by the presence of the 2 m thick fill unit and the interaction between the fill and column head and shaft. In addition, the ground improvement effect on the Coode Island Silt due to the installation of an array of full-displacement columns has likely improved the strength characteristics and reduced the compressibility of this unit (while acknowledging that it is extremely difficult to quantify this "*ground improvement effect*" based on the currently available knowledge of pile/column installation effects). While these various factors introduce uncertainty into the assessment of the rate of sub-soil settlement, there is sufficient data available (Ervin 1992, Srithar 2010) over much of the Yarra Delta to suggest that in the long term, sub-soil support provided by the Coode Island Silt cannot be relied upon. This is due to its long-term measured rate of creep settlement which occurs under little or no applied stress. Loss of subsoil support is, therefore, expected to occur for this embankment.

On this basis, the maximum sag of the geogrid can be calculated by ensuring load compatibility between the stresses acting on the area between columns (a variable which is a function of geogrid deflection) and geogrid tensile load. This is calculated based on the square unit cell shown in Fig. 12 with the tensile load and stiffness in the geogrid calculated as follows:

$$[3] \qquad \text{Tensile load T (kN)} = \frac{\sigma_v(s^2 - a^2)}{4a}\sqrt{1 + \frac{1}{6\varepsilon}}$$

$$[4] \qquad \text{Stiffness J (kN/m)} = \frac{T}{\varepsilon}$$

where s and a are geometric variables, centre-to-centre spacing and width of square column cap respectively, ε is geosynthetic strain and σ_v is the stress acting in the area between columns assessed from the predicted GRC in Fig. 13 and the maximum deflection calculated from Eqn. [2]. The

587 stiffness of the geogrid layer installed is 2600 kN/m (Supplementary Material Section[1]) and in this
588 analysis, it is assumed that the sub-soil settlement is equal to the maximum sag. The results of this
589 analysis are presented in Fig. 16a and b in terms of settlement required and stiffness required for
590 equilibrium respectively. This analysis shows for example that when σ_v = 8 kPa (Fig. 13), the
591 installed geogrid layer would need to settle 87 mm to achieve equilibrium. At present the geogrid
592 settlement is estimated to be about 30 mm. Alternatively, the analysis can be considered in terms of a
593 required stiffness, at relative displacement = 4 %, σ_v = 8 kPa and the geogrid deflection of 57 mm, the
594 geogrid layer would need a stiffness in excess of 10,000 kN/m. From Fig. 16, it can be seen that
595 equilibrium is achieved in the load recovery phase at relative displacement = 7 %, stress reduction
596 ratio = 0.14 (10.1 kPa) and with the maximum geogrid sag of 100 mm, ε = 1.31 % and T = 34.5 kN/m.
597 Whilst designing the geogrid layer to limit the deflection to within the range of maximum arching (2 %
598 < relative displacement < 4 %) may seem like an efficient approach; Fig. 16b indicates that the
599 geogrid layer required would need to be of an extremely high stiffness to limit deflection to within
600 this 30 mm to 60 mm range.

601 Based on the development of arching stresses predicted by the GRC for Area #2 and the
602 analysis presented, four phases of LTP behaviour occurring over the design life of the embankment
603 are proposed (Fig. 17). To date only Phase 1 has been fully observed, the embankment is currently in
604 Phase 2 with the Phase 3 and 4 predicted to occur over the design life of the embankment. The
605 transition from Phase 2 to Phase 3 is predicted to occur in about year 2020 and a working tensile
606 strain of 1.3 % is predicted to develop in about year 2028 at the end of Phase 3 (sub-soil settlement of
607 100 mm). The rate of sub-soil settlement under the current applied stress is due to creep settlement
608 which has been estimated based on a lower bound rate of creep settlement of 5 mm/year based on data
609 presented by Ervin (1992). The creep strain occurring in the geogrid layers during Phase 4 can be
610 calculated from the manufacturer's isochronous curves describing the long term tensile strength-
611 strain-time relationship. The tensile load at the end of Phase 3, is calculated to be 15 % of the mean
612 ultimate tensile strength. The creep induced tensile strain which is predicted during Phase 4 (85 years)

[1] Supplementary data are available with the article through the journal Web site at (**link**)

is calculated to be approximately 0.5 % and the end of design life strain is predicted to be approximately 1.8 % with a maximum geogrid deflection of 117 mm. No attempt has been made here to assess the concentration of tensile strain in the geogrid near the edge of the column head, the values of tensile strain are presented using a simplified analysis to highlight how the development of arching stress affects the geogrid layers, the predicted values of tensile strain are approximate only. It is the intention of this research project to continue with long term monitoring of the LTP behaviour to observe the predicted phases of arching development.

Comparison with design methods

This section compares the observed results and predicted arching stress based on the GRC method with the methods of Zaeske (2001) and van Eekelen *et al.* (2013). These three methods use the same material parameter inputs (γ_{bulk} and ϕ') and similar geometric inputs (s, a and h). The stresses acting in the area between the columns have been converted to a stress reduction ratio value (stress divided by overburden pressure of 74 kPa) and shown in Fig. 18. The three methods predict a value of stress reduction ratio within a reasonably small range of between 0.06 and 0.10, with the GRC and the method of Van Eekelen showing good agreement with the measured data at maximum arching. As both the method of Zaeske and Van Eekelen are derived independent of sub-soil settlement, the calculated values of stress reduction ratio are constant with respect to time and sub-soil settlement. For the purpose of design, a constant "design" value of stress acting on the geogrid in the area between columns may be appropriate, provided of course that this value is representative, and on the safe side, of the ultimate stress acting on the geogrid layer through its' design life.

However, unlike other common methods, the GRC method has the ability to describe the development of arching stresses through the design life of the embankment. Most importantly, the development of arching stresses described by the GRC (Fig. 17) implies that adopting a design stress for the geogrid based on maximum arching is not conservative unless:

(1) the geogrid is designed to limit deflection to a value of relative displacement less than 4 %, this requires a geogrid layer of very high stiffness and in most cases will not be feasible,

639 or (2) design assumes long term sub-soil support which limits relative displacement to less
640 than 4 % (which requires knowledge of the long term sub-soil performance and more
641 importantly an understanding of how arching stresses develop).

642 The analysis presented suggests that the stress acting on the geogrid layer in Phase 3 is
643 approximately 50 % larger than that acting during maximum arching (Phase 2). As a result, designing
644 the geogrid layer based on an arching model that predicts stresses at maximum arching and/or on the
645 basis of stresses observed shortly after the completion of embankment construction, where maximum
646 arching is likely to be occurring, may result in geogrid that is under-designed in the long term.

647 Further evidence of GRC behaviour in field studies

648 Field scale studies that have observed sub-soil settlement and arching stresses simultaneously are
649 quite limited. The most conclusive data showing the arching stress development as a function of sub-
650 soil settlement at field scale comes from the TH 241 embankment near St. Michael, Minnesota, USA
651 (Wachman and Labux 2008). The vertical stress measured at the base of the LTP over a 250 day
652 period show the characteristic features of the GRC; initial, maximum and load recovery phases of
653 arching as proposed herein. The authors have indicated the phases of arching development on the
654 original data[1] reported by Wachman and Labux (2008) (Fig. 19a). The arrangement of the EPCs and
655 triangular grid layout of columns is shown in Fig. 19b.

656 In a separate field case study, van Eekelen et al (2010) presented instrumentation data
657 recorded over a 3.5 year period for the Kyoto Road embankment project in the Netherlands. The
658 authors, similar to the above case, have indicated the inferred periods of arching development (initial,
659 maximum arching and load recovery phase) on the original data which describes the vertical stress
660 acting on the sub-soil (load component C) (Fig. 20a). This data highlights that over the long-term the
661 stresses at acting maximum arching do not represent the long-term arching stresses that will prevail
662 over the remaining design life of this embankment. The layout of the columns, arrangement of the
663 EPCs, a method used to assess sub-soil stress by van Eekelen *et al.* (2010) is shown in Fig. 20b.

[1] The original data has been reproduced in Fig. 19 as a trendline through the original datapoints

Discussion

The field data and analysis presented above is not without limitations inherent to most field scale studies. In this case they include: (a) variability of the sub-surface conditions, particularly the fill unit and settlement characteristics of the Coode Island Silt, and (b) the effects of the upper level ground improvement works on a partially constructed embankment introduces uncertainty and limits the extent to which the LTP behaviour can be accurately analysed. However, this uncertainty primarily relates to the assessment of the sub-soil settlement and assessing when the various phases of arching will occur. Based on the field data of Wachman and Labuz (2008) and van Eekelen et al (2010) described above as well as extensive laboratory testing which have observed maximum arching (Terzaghi 1936; Ladanyi and Hoyaux 1969; Evans 1983; Iglesia *et al.* 1999, 2013, Chen *et al* 2008; Ellis and Aslam 2009a, 2009b), the authors consider that there is sufficient evidence to suggest that the load recovery phase will occur. However, it is difficult to assess precisely when this will occur.

The prediction that stress acting on the geosynthetic reinforcement will begin to increase over the long term has considerable importance in LTP design. It has been shown that the geosynthetic layer must have an unrealistically high stiffness in order to achieve equilibrium at maximum arching stresses and as a result, in most cases, equilibrium between stress acting between the columns and the geosynthetic layer will occur in the load recovery phase unless the sub-soil support is provided. For this particular case study, extensive data is available (see Ervin 1992) which indicates that significant long-term settlement of the Coode Island Silt can be expected under small or zero applied stress. As a result, sub-soil support is unlikely to be permanent over the design life of the embankment. The authors consider that the reliance on sub-soil support in (ultimate limit state) design is problematic given that the arching stress development in the load recovery phase occurs under a positive feedback loop (i.e., increasing settlement will lead to increasing stress leading to further settlement, etc.). In addition, creep induced settlement is often significant for road and rail embankments which typically have a design life in the order of 100 years. The “equilibrium” conditions which establish shortly after embankment completion, at maximum arching and with sub-soil support, are not likely to prevail over

690 the design life of the embankment in many cases and may not be representative of the ultimate limit
691 state.

692 A design of the geosynthetic layer based on the value of stress in the area between columns
693 achieved under equilibrium conditions with no sub-soil support in the load recovery phase (see Fig.
694 17c), is in the authors opinion, a prudent ultimate limit state design value which the geosynthetic layer
695 can be designed to resist. The design approach outlined in this paper and summarised in Fig. 17
696 differs from the widely adopted "2-step" design approach found in various design standards (EBGEO
697 2010, BS8006 2011 and CUR2015) where an arching model is used to calculate the stress acting in
698 the area between columns in Step 1 independent of sub-soil settlement, and in Step 2, the stress in the
699 area between columns from Step 1 is used to assess geosynthetic behaviour. This "2-step" approach is
700 at odds with the coupled relationship between arching stresses and sub-soil settlement highlighted in
701 this paper. Furthermore, the constant values of arching stresses predicted by the limit equilibrium
702 models provide little insight into the phases of arching development described by the GRC (initial,
703 maximum and load recovery phase) that have been outlined in this paper. The authors consider that
704 the concept of arching development in phases (Fig. 17), provides knowledge that would be highly
705 beneficial to designers and is important for understanding the development of arching stresses, the
706 interaction with the geosynthetic reinforcement and the overall behaviour of a load transfer platforms.

707 Much of the analysis presented above focuses on assessing the stresses acting in the area
708 between columns for ultimate limit state design of the geogrid. Another equally important
709 consideration is the impact on embankment deformations as these phases of arching development
710 occur. A common feature observed in many field case studies, and shown here also, is sub-soil
711 settlement occurring for a considerable period post-construction. For the case study presented here,
712 the sub-soil settlement is predicted to increase from the present value of about 50 mm to about 100
713 mm as phase 2 and 3 occur over the next 12 years (Fig. 17). For the case study considered here this is
714 not expected to adversely affect rail performance due to the height of the embankment. However, the
715 authors consider that this behaviour has considerable implications for shallow height embankments
716 where this continuing sub-soil settlement may lead to surface deformation.

The authors recommend that further development of arching models for the purpose of load transfer platform design should incorporate sub-soil settlement as a governing parameter. While the GRC method describes these phases, further validation of the GRC method with various geometric and material properties is required. In particular, the properties characterising the GRC and developed based on the 2D trapdoor tests, require validation (or otherwise) based on 3D column-supported embankment tests. In the author's opinion, the GRC parameters (Fig. 11) of interest include: the empirically derived initial and secant arching modulus values of 63 and 125 respectively, the relative displacement range of maximum arching (2 % < relative displacement < 4 %), the relative displacement range at which maximum arching transitions to the load recovery phase (3 % < relative displacement < 5 %), and finally, how the equivalent relative displacement is assessed (i.e., is it assessed based on the settlement at the edge of the column head, or the displacement where maximum sag occurs (as assumed here), or is there some other value representative of the sub-soil settlement that should be used?) The results of the analysis presented in this paper suggest that the characteristic parameters of the GRC are, at the least, reasonable for describing the 3D arching associated with column-supported embankments, however further validation is required.

Conclusion

The instrumentation of a GRCSE in Melbourne, Australia has been undertaken with over 2 years of post-construction data presented. The measured data has shown the time-dependent development of arching stresses during the post-construction period and it has been further demonstrated, through analysis of the data, that this behaviour is due to the sub-soil settlement in the area between columns. The relationship between arching stresses and sub-soil settlement has been observed previously in laboratory trapdoor tests (Terzaghi 1936; Ladanyi and Hoyaux 1969; and Evans 1983 amongst others), small-scale centrifuge trapdoor models (Iglesia *et al.* 2011, 2013), column-supported embankment centrifuge models (Ellis and Aslam 2009a, 2009b) and small scale column-supported embankments (Chen *et al.* 2008) and is shown here at field scale. Reasonably good predictions of the stress reduction ratio at maximum arching have been made based on the method of Zaeske (2001), van Eekelen *et al.* (2013) and with the GRC method.

744 However, it has been shown that the GRC method can describe the development of arching
745 stresses from initial arching to maximum arching, and in addition, has been used to predict the
746 development of arching stresses in the future. The concept of the arching development described by
747 an initial, maximum and load recovery phase is a concept that the authors consider to be particularly
748 useful in understanding LTP behaviour and one which would greatly benefit designers. The load
749 recovery phase is the phase of most importance for LTP design. The concept that the arching stresses
750 begin to break-down in the long term with increasing sub-soil settlement has been shown to occur in
751 embankment field case studies (Wachman and Labuz 2008; van Eekelen et al. 2010), in extensive
752 laboratory testing used to develop the GRC method (see Iglesia 1991) and by a limited number of
753 researchers investigating column-supported embankments (Chen *et al.* 2008; Ellis and Aslam 2009a,
754 2009b). This has important implication for the design of the geogrid layer, and perhaps more
755 importantly, has considerable implication concerning long-term embankment performance,
756 particularly concerning surface settlement of shallow height embankments.

757 While the GRC and the concept of arching development in phases have been discussed
758 previously by others, given the implications highlighted in this paper, the authors consider that further
759 research into the role of sub-soil settlement in the development of arching stresses, and particularly
760 the load recovery phase, is warranted.

761 ## Acknowledgments

762 The lead author would like to thank Golder Associates ("Innovation and Excellence" (i2x)
763 award) and Monash University for the financial assistance and support provided to pursue his Ph.D.
764 studies. We are grateful to the Regional Rail Link – City to Maribyrnong River (RRLCMR) Alliance
765 for supporting and providing the opportunity to undertake this field case study. In addition, the design
766 support provided by the RRLCMR Alliance to obtain the necessary approvals and their assistance
767 during the construction and instrumentation installation phases is greatly appreciated. Testing of the
768 geogrid was performed at TRI Australasia's geosynthetics laboratory in Burleigh Heads, QLD,
769 Australia. The authors would like to thank Warren Hornsey for allowing the use of these facilities.

770

771 ## References

772

773 AS. 2007. Australian Standard - Method of testing soils for engineering purposes Method 5.8.1: Soil
774 compaction and density tests - determination of field density and field moisture content of a soil
775 using a nuclear surface moisture - density gauge - direct transmission mode (AS 1289.5.8.1-
776 2007). SAI Global. Sydney, NSW, Australia.
777 Aslam, R. and Ellis, E. A. 2008. Centrifuge modelling of piled embankments. *In* Proceedings of the
778 1st International Conference on Transportation Geotechnics - Advances in Transportation
779 Geotechnics, Nottingham, U.K., 25-27 August 2008. CRC Press, pp. 363-368.
780 Briançon, L. and Simon, B. 2011. Performance of pile-supported embankment over soft soil: full-
781 scale experiment. Journal of Geotechnical and Geoenvironmental Engineering, **138**(4): 551-561
782 BS8006-1. 2010. Code of Practice for Strengthened/Reinforced Soils and Other Fills. British
783 Standards Institution. London, UK.
784 Bathurst, R. J., Allen, T. M., and Walters, D. L. 2002. Short-term strain and deformation behavior of
785 geosynthetic walls at working stress conditions. Geosynthetics International, **9**(5-6): 451-482.
786 Chen, Y.-M., Cao, W.-P., and Chen, R.-P. 2008. An experimental investigation of soil arching within
787 basal reinforced and unreinforced piled embankments. Geotextiles and Geomembranes, **26**(2):
788 164-174. doi: 10.1016/j.geotexmem.2007.05.004
789 Costa, Y. D., Zornberg, J. G., Bueno, B. S., and Costa, C. L. 2009. Failure mechanisms in sand over a
790 deep active trapdoor. Journal of Geotechnical and Geoenvironmental Engineering, **135**(11): 1741-
791 1753
792 Cupper, M. L., White, S., and Neilson, J. L. 2003. Quaternary: Ice Ages - environments of change, *in*
793 Geology of Victoria. Edited by W. D. Birch, Geological Society of Australia, pp. 337-359.
794 CUR226 2010. Ontwerprichtlijin paalmatrassyststemen (Design Guideline Piled Embankments, ISBN
795 978-90-376-0518-1 (in Dutch).
796 CUR226 2015. Ontwerprichtlijin paalmatrassyststemen (Design Guideline Piled Embankments)
797 updated version, to be published in 2015 (in Dutch).
798 Dewoolkar, M. M., Santichaianant, K., and Ko, H.-Y. 2007. Centrifuge modeling of granular soil
799 response over active circular trapdoors. Soils and Foundations, **47**(5): 931-945
800 EBGEO. 2010. Recommendations for Design and Analysis of Earth Structures Using Geosynthetic
801 Reinforcements - EBGEO (2011). Translation of the 2nd German edition. German Geotechnical
802 Society. Ernst & Sohn. Germany.
803 Ellis, E., and Aslam, R. 2009a. Arching in piled embankments: comparison of centrifuge tests and
804 predictive methods - Part 1 of 2. Ground Engineering, **42**(6): 34-38
805 Ellis, E., and Aslam, R. 2009b. Arching in piled embankments: comparison of centrifuge tests and
806 predictive methods - Part 2 of 2. Ground Engineering, **42**(7): 28-31
807 Ervin, M. C. 1992. Engineering properties of Quaternary age sediments of the Yarra Delta: *In*
808 Engineering Geology of Melbourne. Edited by W.A. Peck, J.L. Neilson, R.J. Olds and K.D.
809 Seddon. Rotterdam, Netherlands, A. A. Balkema. pp. 245-259.
810 Evans, C. H. 1983. An examination of arching in granular soils. M.Sc. thesis, Department of Civil
811 Engineering, Massachusetts Institute of Technology, Cambridge, MA.
812 Filz, G., Sloan, J., McGuire, M. P., Collin, J., and Smith, M. 2012. Column-Supported Embankments:
813 Settlement and Load Transfer. *In* Proceedings of the Geotechnical Engineering State of the Art
814 and Practice - Keynote Lectures from GeoCongress 2012. ASCE, pp. 54-77.

Giroud, J. P. 1995. Determination of geosynthetic strain due to deflection. Geosynthetics International, **2**(3): 635-641. doi: 10.1680/gein.2.0028

Gniel, J., and Haberfield, C. 2015. Design, construction and performance of a tied-wall embankment supported on concrete column ground improvement. *In* Proceedings of the Proceedings of the International Conference on Geotechnical Engineering: Soil-Structure Interaction, Underground Structures and Retaining Walls St. Petersburg, Russia, June 2014. IOS Press, pp. 18-27.

Haberfield, C. M., and Szymakowski, J. 2003. Applications of large scale direct shear testing. Australian Geomechanics, **38**(1): 29-39

Haring, W., Profittlich, M., and Hangen, H. 2008. Reconstruction of the national road N210 Bergambacht to Krimpen a.d. IJssel, NL: design approach, construction experiences and measurement results. *In* Proceedings of the 4th European Geosynthetics Conference, Heriot-Watt University, Edinburgh, U.K., 7-10 September 2008

Hewlett, W. J., and Randolph, M. 1988. Analysis of piled embankments. Ground Engineering, **21**(3): 12-18

Iglesia, G. R. 1991. Trapdoor Experiments on the Centrifuge--a Study of Arching in Geomaterials and Similitude in Geotechnical Models Massachusetts Institute of Technology, Department of Civil Engineering.

Iglesia, G. R., and Einstein, H. H. 2015. Closure to "Investigation of Soil Arching with Centrifuge Tests" by Geraldo R. Iglesia, Herbert H. Einstein, and Robert V. Whitman. Journal of Geotechnical and Geoenvironmental Engineering: 07015010

Iglesia, G. R., Einstein, H. H., and Whitman, R. V. 1999. Determination of vertical loading on underground structures based on an arching evolution concept. *In* Proceedings of the 3rd National Conference - Geo-Engineering for Underground Facilities, University of Illinois, Urbana-Champaign, Illinois, June 13-17 1999, pp. 495-506.

Iglesia, G. R., Einstein, H. H., and Whitman, R. V. 2011. Validation of Centrifuge Model Scaling for Soil Systems via Trapdoor Tests. Journal of Geotechnical and Geoenvironmental Engineering, **137**(11): 1075-1089. doi: 10.1061/(ASCE)GT.1943-5606.0000517

Iglesia, G. R., Einstein, H. H., and Whitman, R. V. 2013. Investigation of Soil Arching with Centrifuge Tests. Journal of Geotechnical and Geoenvironmental Engineering, **140**(2). doi: 10.1061/(ASCE)GT.1943-5606.0000998

Jacobsz, S. 2016. Trapdoor experiments studying cavity propagation. In Proceedings of the 1st Southern African Geotechnical Conference, Durban, South Africa, October 18-19 2016. CRC Press, pp. 159-165.

Jefferies, M., and Been, K. 2006. Soil liquefaction: a critical state approach, 2nd edition. CRC Press.

King, D. J. 2017. The behaviour of geosynthetic reinforced embankments with semi-rigid ground improvement (not submitted). Ph.D. thesis, Department of Civil Engineering, Monash University, Melbourne, Australia.

King, D. J., Bouazza, A., Gniel, J., and Bui, H. H. 2016. The compressibility, permeability and structured nature of the Coode Island Silt. Australian Geomechanics, **50**(2): pp. 45-65

King, D. J., Gniel, J., Bouazza, A., Ha, H. H., and Rowe, R. K. 2014. Preliminary observations from a geosynthetic reinforced piled embankment. *In* Proceedings of the 10th International Conference on Geosynthetics, Berlin, Germany. German Geotechnical Society, Essen, Germany

Ladanyi, B., and Hoyaux, B. 1969. A study of the trap-door problem in a granular mass. Canadian Geotechnical Journal, **6**(1): 1-14

Lawson, C. R. 2012. Role of modelling in the development of design methods for basal reinforced piled embankments. *In* Proceedings of the EuroFuge 2012, Delft, Netherlands, April 23-24 2012. Delft University of Technology and Deltares, Netherlands

Liu, K.-W., and Rowe, R. K. 2015. Numerical study of the effects of geosynthetic reinforcement viscosity on behaviour of embankments supported by deep-mixing-method columns. Geotextiles and Geomembranes, **43**(6): 567-578

Lowe, J. 1964. Shear strength of coarse embankment dam materials. *In* Proceedings of the 8th International Congress on Large Dams, Edinburgh, Scotland. International Commission on Large Dams, pp. 745-761.

Lunne, T., Robertson, P. K., and Powell, J. J. M. 1997. Cone Penetration Testing in Geotechnical Practice. Blackie Academic, EF Spon/Routledge, New York.

McGuire, M. P., and Filz, G. M. 2008. Quantitative comparison of theories for geosynthetic reinforcement of column-supported embankments. *In* Proceedings of the 1st Pan American Geosynthetics Conference and Exhibition, Cancun, Mexico, 1-5 March 2008, pp. 1303–1312.

Naughton, P. J., and Kempton, G. T. 2005. Comparison of analytical and numerical analysis design methods for piled embankments. *In* Proceedings of the Geo-Frontiers 2005 Congress, Austin, Texas, 24-26 January 2005. ASCE Geotechnical Special Publication (GSP) 130-142, Reston, VA

Neilson, J. L. 1992. Geology of the Yarra Delta: *In* Engineering Geology of Melbourne. W.A. Peck, J.L. Neilson, R.J. Olds and K.D. Seddon. (eds.). Rotterdam, Netherlands, A. A. Balkema. pp. 223-245.

Oglesby, J. W., Mahmoodzadegan, B., and Griffin, P. M. 1992. Evaluation of methods and materials used to attach strain gages to polymer grids for high strain conditions. Louisiana Transportation Research Center. Baton Rouge, LA.

Ono, K., and Yamada, M. 1993. Analysis of the arching action in granular mass. Géotechnique, **43**(1): 105-120. doi:10.1680/geot.1993.43.1.105

Rowe, R. K., and Liu, K.-W. 2015. Three-dimensional finite element modelling of a full-scale geosynthetic-reinforced, pile-supported embankment. Canadian Geotechnical Journal, **52**(12): 2041-2054

Shinoda, M., and Bathurst, R. J. 2004. Strain measurement of geogrids using a video-extensometer technique. Geotechnical Testing Journal, **27**(5): 456-463. doi: 10.1520/GTJ11940

Srithar, S. T. 2010. Settlement characteristics of Coode Island Silt. Australian Geomechanics, **45**(1): 55-64

Stone, K. J. L. 1988. Modelling of rupture development in soils. Ph.D. thesis, Department of Civil Engineering, University of Cambridge, Cambridge, U.K.

Stone, K. J. and Wood, D. M. 1992. Effects of dilatancy and particle size observed in model tests on sand. Soils and Foundations, 32(4): 43-57.

Terzaghi, K. 1936. Stress distribution in dry and in saturated sand above a yielding trap-door.

Terzaghi, K. 1943. Theoretical Soil Mechanics. John Wiley and Sons, New York.

van Eekelen, S. J. M., and Bezuijen, A. 2012a. Does a piled embankment 'feel'the passage of a heavy truck? High frequency field measurements. *In* Proceedings of the 5th European Geosynthetics Congress (EuroGeo5), Valencia, Spain, 16-19 September 2012, pp. 162-166.

van Eekelen, S. J. M., Bezuijen, A., and Alexiew, D. 2010. The Kyoto road piled embankment: 3.5 years of measurements. *In* Proceedings of the 9th International Conference on Geosynthetics, Guaruja, Brazil, 23-27 May 2010, pp. 1941-1944.

van Eekelen, S. J. M., Bezuijen, A., Lodder, H. J., and van Tol, A. F. 2012b. Model experiments on piled embankments. Part I. Geotextiles and Geomembranes, **32**: 69-81. doi: 10.1016/j.geotexmem.2013.07.005

van Eekelen, S. J. M., Bezuijen, A., Lodder, H. J., and van Tol, A. F. 2012c. Model experiments on piled embankments. Part II. Geotextiles and Geomembranes, **32**: 82-94. doi: 10.1016/j.geotexmem.2013.07.005

van Eekelen, S. J. M., Bezuijen, A., and van Tol, A. F. 2013. An analytical model for arching in piled embankments. Geotextiles and Geomembranes, **39**: 78-102. doi: 10.1016/j.geotexmem.2013.07.005

van Eekelen, S., Bezuijen, A. & Van Tol, A. (2015) Validation of analytical models for the design of basal reinforced piled embankments. *Geotextiles and geomembranes* **43**(1):56-81

Vardoulakis, I., Graf, B. and Gudehus, G. 1981. Trap-door problem with dry sand: a statical approach based upon model test kinematics. International Journal for Numerical and Analytical Methods in Geomechanics, **5**(1): 57-78

Wachman, G., and Labuz, J. 2008. TH 241 column-supported embankment. Department of Civil Engineering, University of Minnesota. Report prepared for the Minnesota Department of Transport, St Paul, Minnesota, U.S.A. 111 p.

Zaeske, D. 2001. Zur Wirkungsweise von unbewehrten und bewehrten mineralischen Tragschichten über pfahlartigen Gründungselementen. Schriftenreihe Geotechnik, Univeristy Kassel, Hesse, Germany.

Zhuang, Y., Ellis, E., and Yu, H. S. 2012. Three-dimensional finite-element analysis of arching in a piled embankment. Geotechnique, **62**(12): 1127-1131. doi: 10.1680/geot.9.P.113

Zhuang, Y., Wang, K. Y., and Liu, H. L. 2014. A simplified model to analyze the reinforced piled embankments. Geotextiles and Geomembranes, **42**(2): 154-165. doi: 10.1016/j.geotexmem.2013.07.005

FIGURE CAPTIONS

Fig. 1. Surface geology of the Yarra Delta (modified from Cupper et al. 2003) with ground improvement zones and approximate extent of RRLCMR alignment shown.

Fig. 2. (a) Embankment long section. Corrected cone tip resistance profiles and soil behaviour type **(b)** CPT29, **(c)** CPT30, **(d)** CPT11 and **(e)** Undrained shear strength s_u profile – various CPTs, vane shear data adjacent to CPT11 from King *et al.* (2016a)

Fig. 3. North Dynon embankment – plan view

Fig. 4. Embankment cross section - Area #2

Fig. 5. Plan view of Instrumentation Area #2

Fig. 6. Embankment construction timeline - Area #2

Fig. 7. EPC data for Area # 2

Fig. 8. EPC data for Stage 3b works in Area #2

Fig. 9. Strain gauge data - Area #2: **(a)** transverse and **(b)** longitudinal

Fig. 10. Stress reduction ratio for Area #2

Fig. 11. Characteristic Ground Reaction Curve (GRC) (modified from Iglesia *et al.* 2011)

Fig. 12. Equivalent unit cell – Area #2

Fig. 13. Predicted GRC – Area #2

Fig. 14. Area #2 – stress reduction ratio based on EPC2 with GRC features

Fig. 15. Maximum deflection of geogrid and sub-soil settlement

Fig. 16. Calculated geogrid equilibrium at loss of sub-soil support (a) required settlement (b) required stiffness

952 **Fig. 17.** Four phases of arching development based on application of GRC method to Area #2 – **(a)**

953 Initial arching **(b)** Maximum arching **(c)** Load recovery **(d)** Creep strain

954 **Fig. 18.** Comparison of arching stresses – various methods

955 **Fig. 19. (a)** EPC data for TH 241 embankment and **(b)** instrumentation layout plan modified from

956 Wachman and Labuz (2008)

957 **Fig. 20.** Kyoto road data, sub-soil stress (modified from van Eekelen, 2010

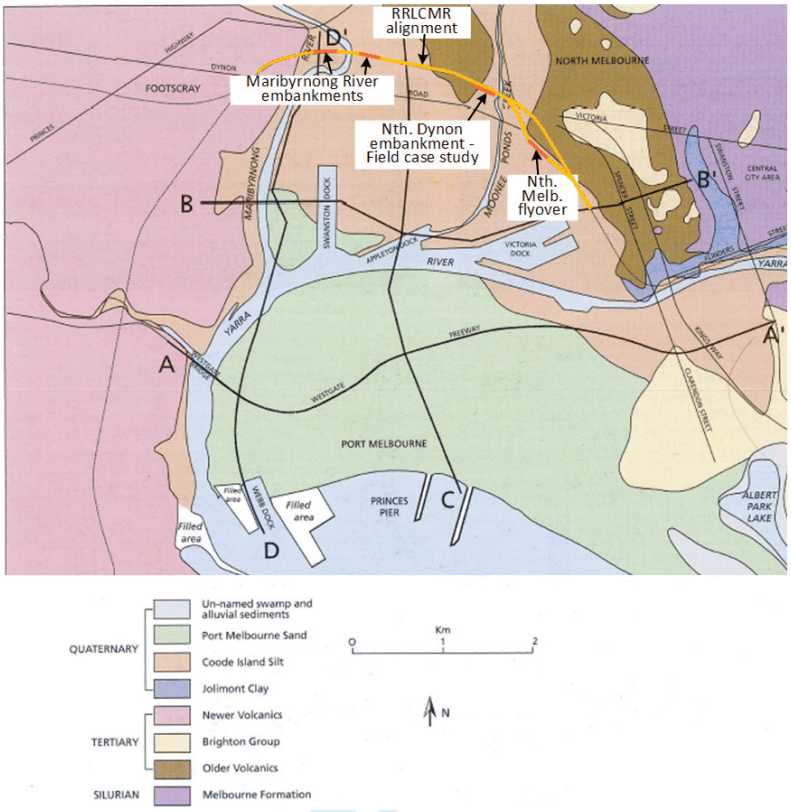

963

964 **Fig. 1.** Surface geology of the Yarra Delta (modified from Cupper et al. 2003) with embankment
965 ground improvement zones and approximate extent of RRLCMR alignment shown.

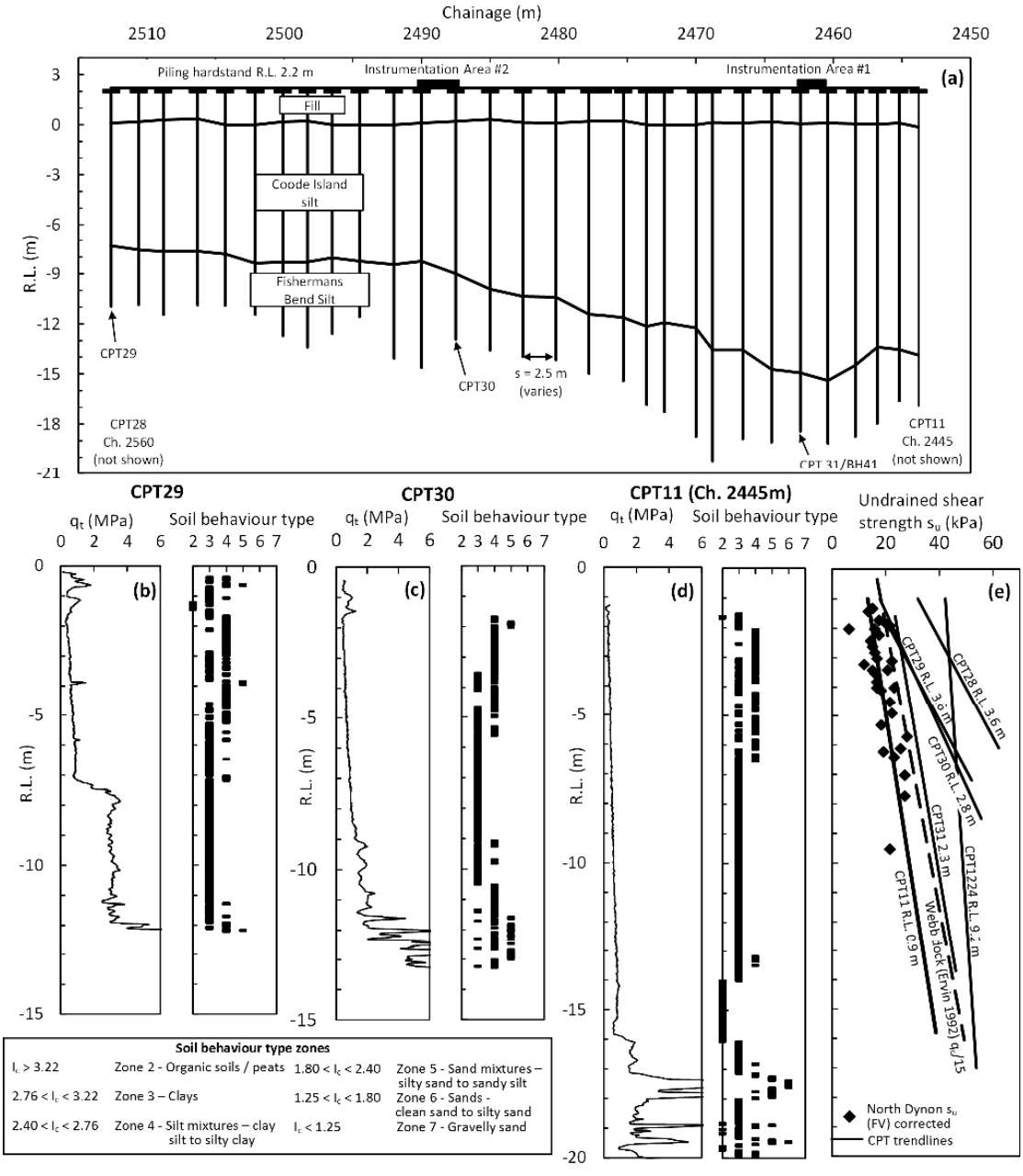

Fig. 2. (a) Embankment long section. Corrected cone tip resistance profiles and soil behaviour type **(b)** CPT29, **(c)** CPT30, **(d)** CPT11 and **(e)** Undrained shear strength s_u profile – various CPTs, vane shear data adjacent to CPT11 from King *et al.* (2016)

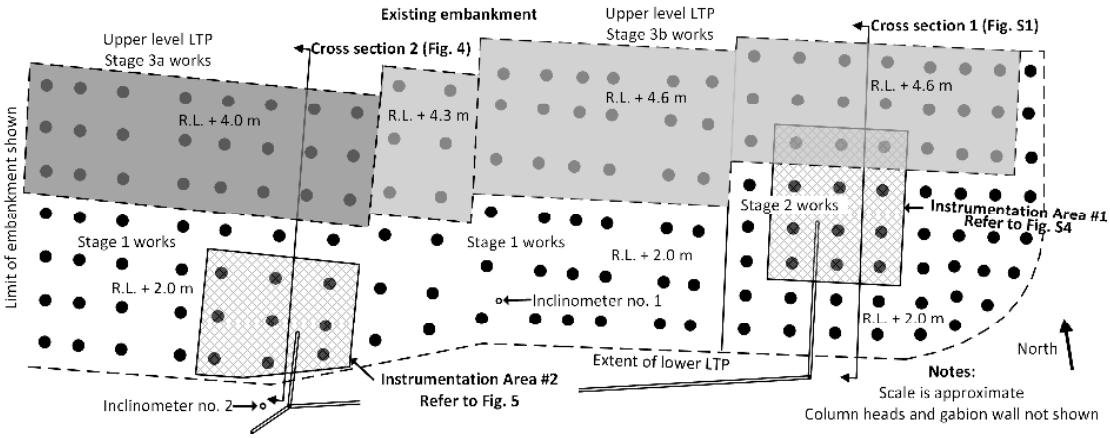

Fig. 3. North Dynon embankment – plan view

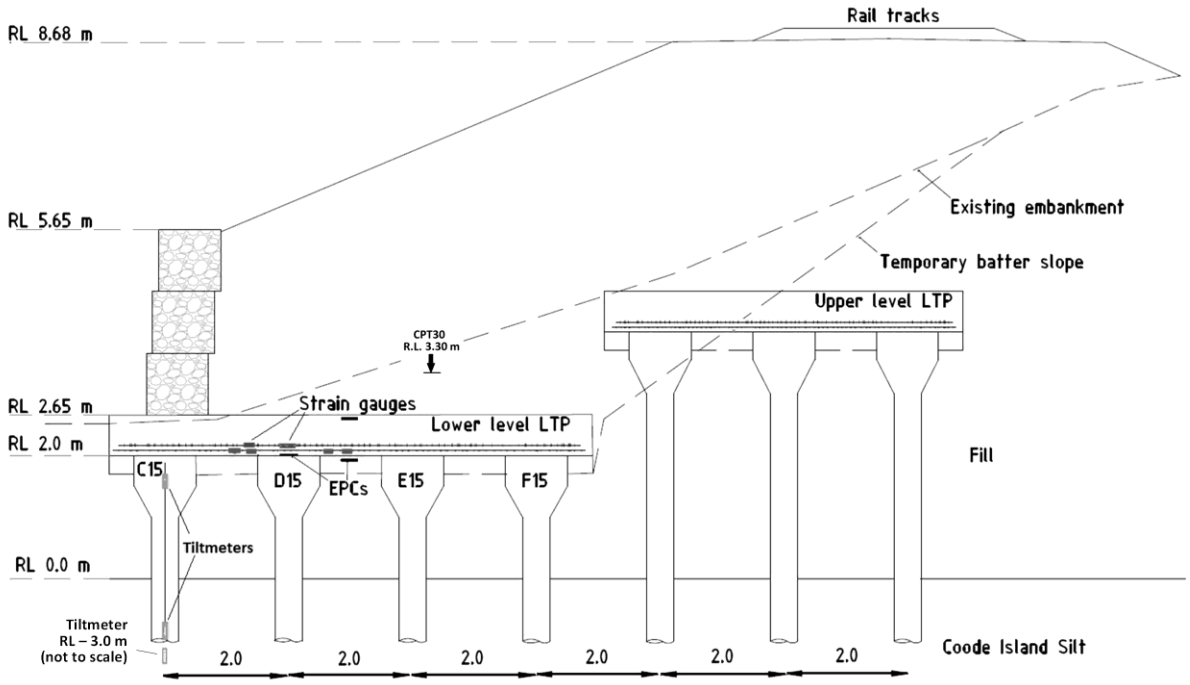

Fig. 4. Embankment cross section - Area #2

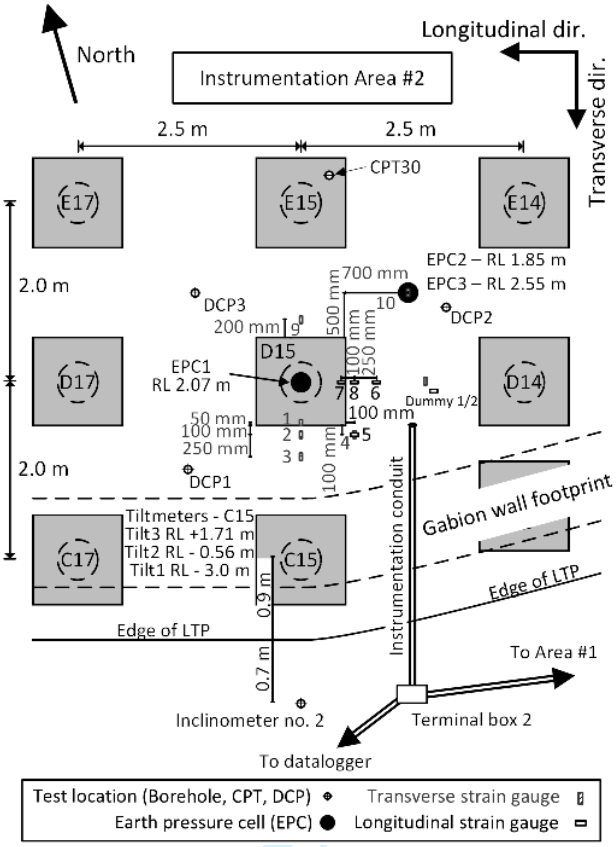

974

975 **Fig. 5.** Plan view of Instrumentation Area #2

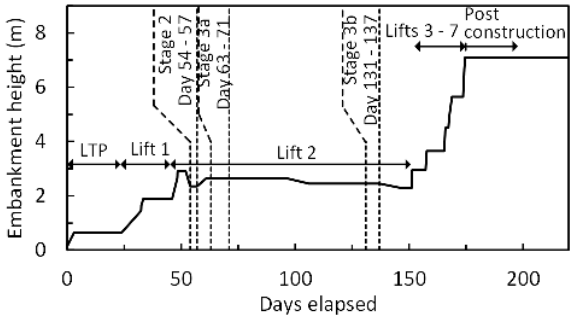

976

977 **Fig. 6.** Embankment construction timeline - Area #2

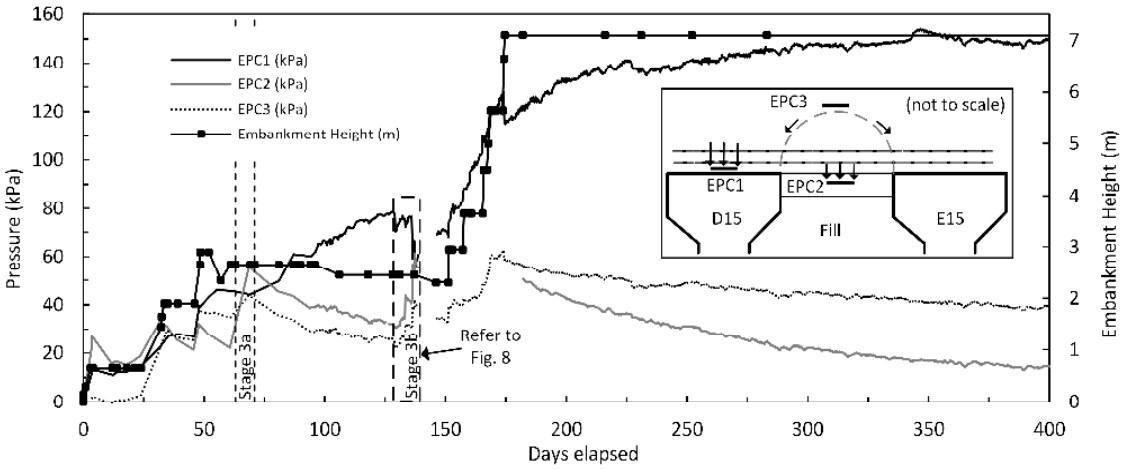

978

979 **Fig. 7.** EPC data for Area # 2

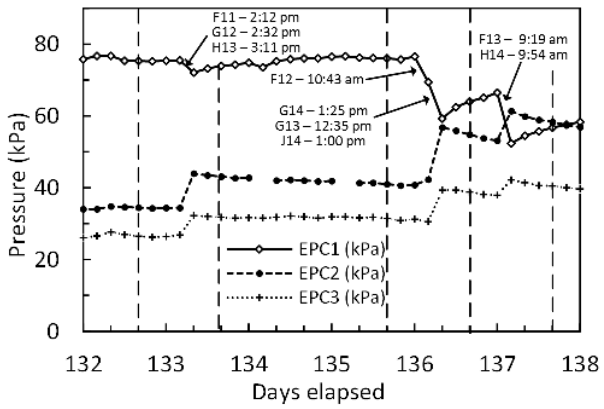

980

981 **Fig. 8.** EPC data for Stage 3b works in Area #2

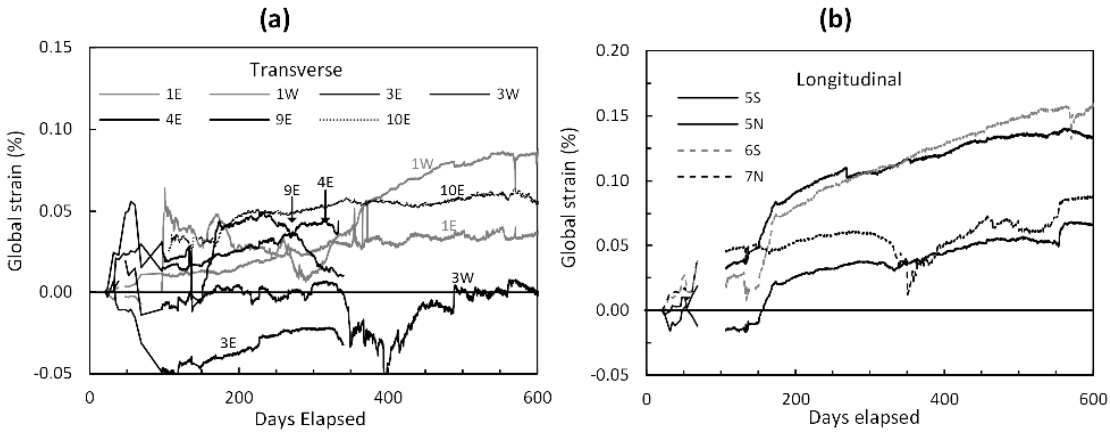

982

983 **Fig. 9.** Strain gauge data - Area #2: **(a)** transverse and **(b)** longitudinal

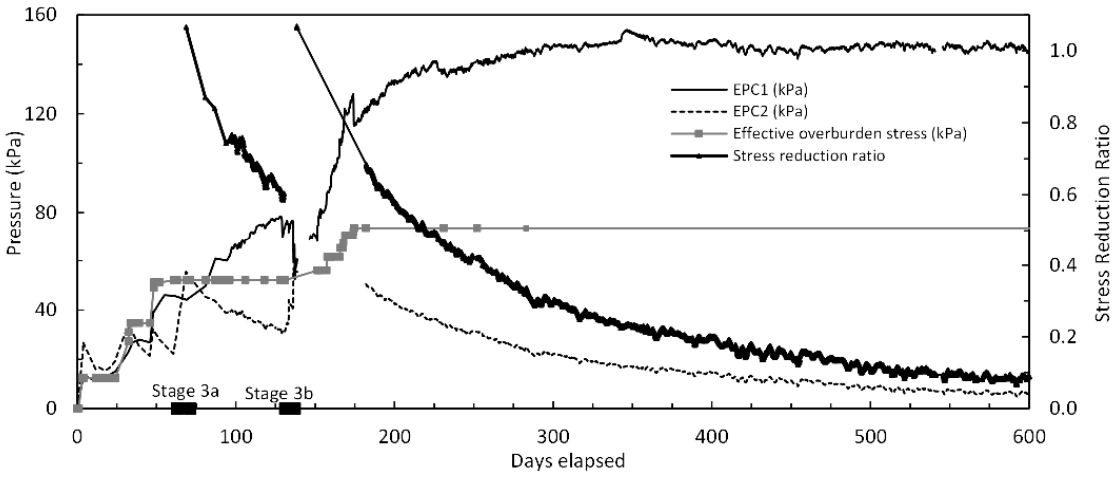

984

985 **Fig. 10.** Stress reduction ratio for Area #2

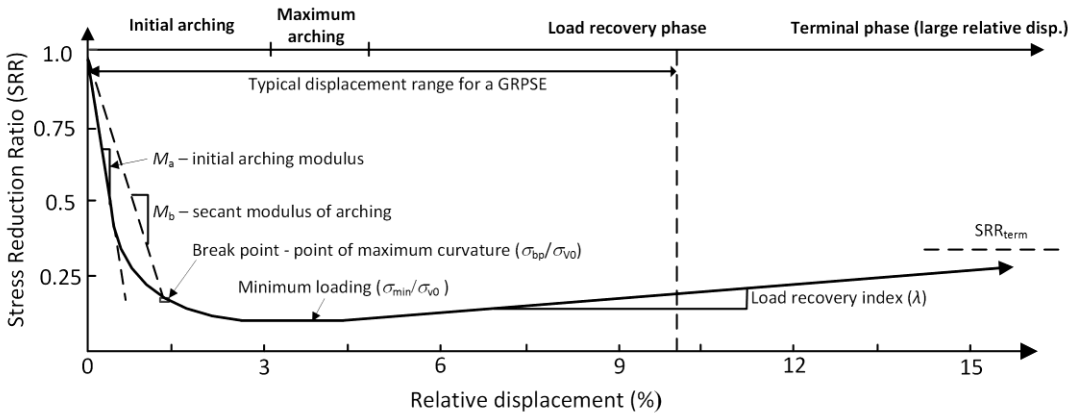

Fig. 11. Characteristic Ground Reaction Curve (GRC) (modified from Iglesia *et al.* 2011)

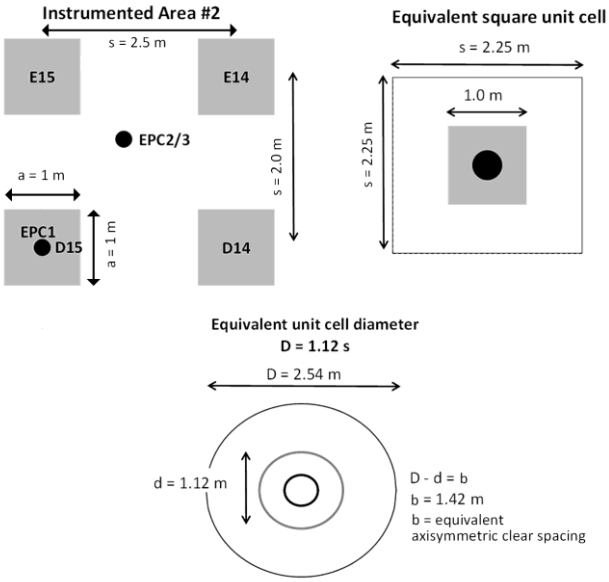

Fig. 12. Equivalent unit cell – Area #2

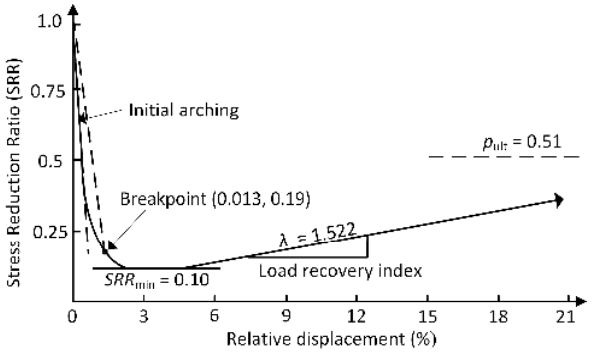

991

992 **Fig. 13.** Predicted GRC – Area #2

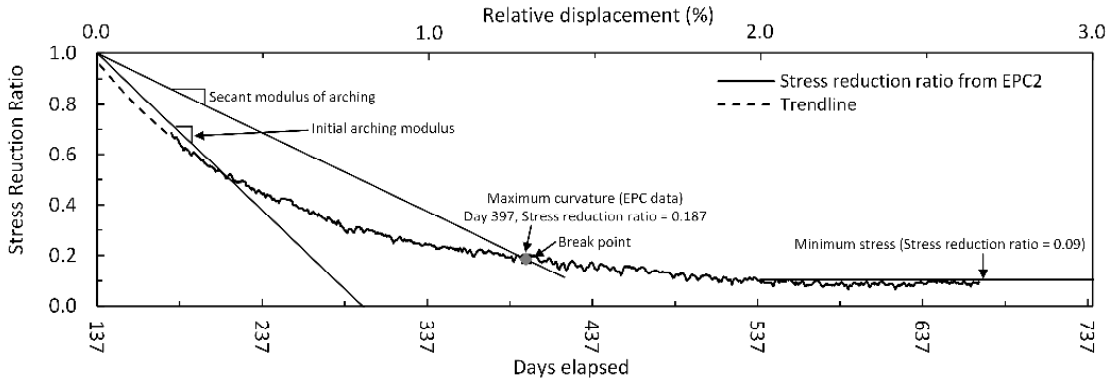

993

994 **Fig. 14.** Area #2 – stress reduction ratio based on EPC2 with GRC features

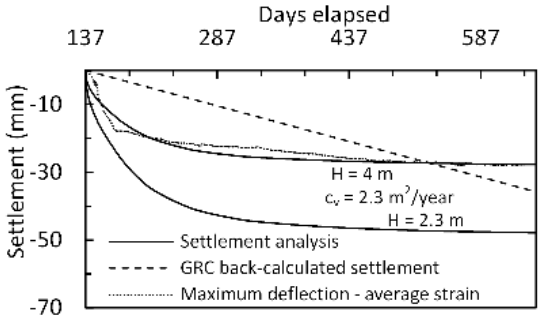

995

996 **Fig. 15.** Maximum deflection of geogrid and sub-soil settlement

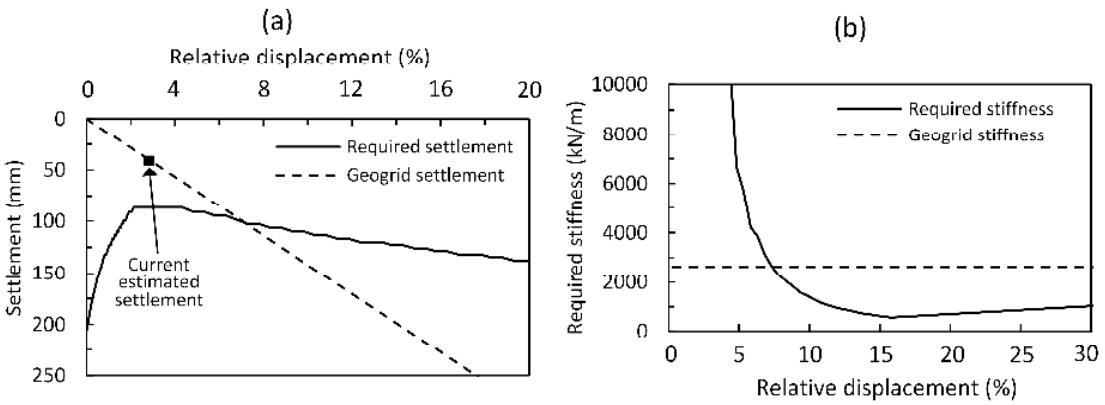

997

998 **Fig. 16.** Calculated geogrid equilibrium at loss of sub-soil support (a) required settlement (b) required
999 stiffness

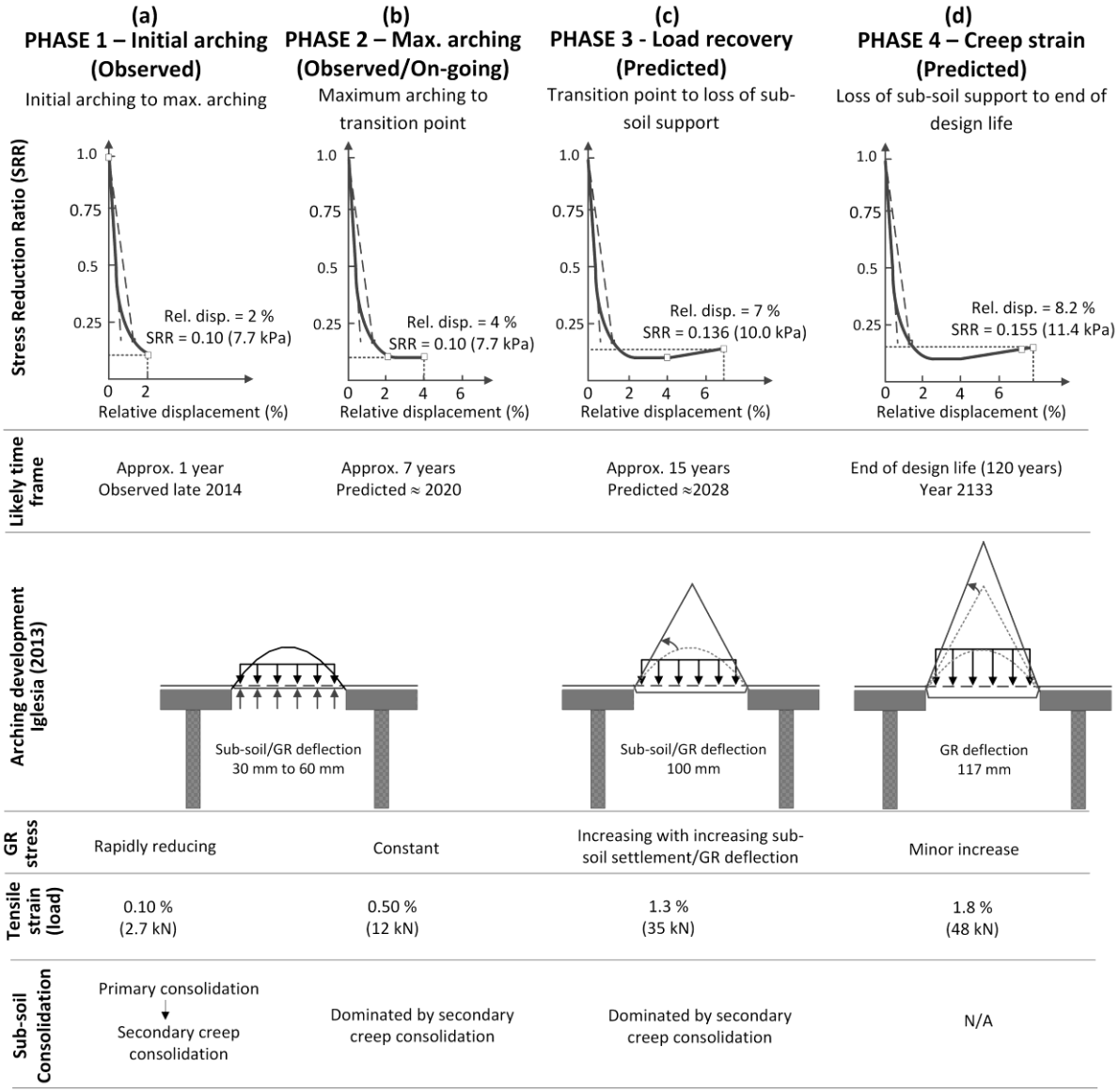

Fig. 17. Four phases of arching development based on application of GRC method to Area #2 – **(a)** Initial arching **(b)** Maximum arching **(c)** Load recovery **(d)** Creep strain

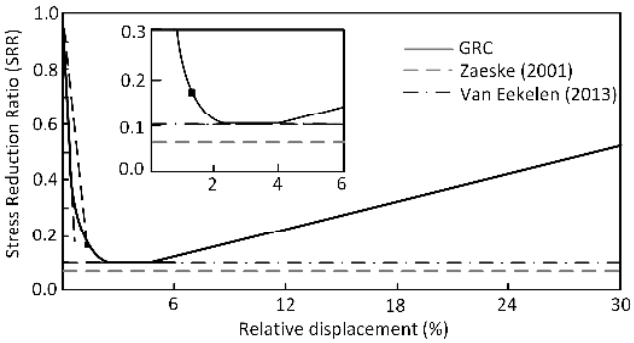

1003

1004 **Fig. 18.** Comparison of arching stresses – various methods

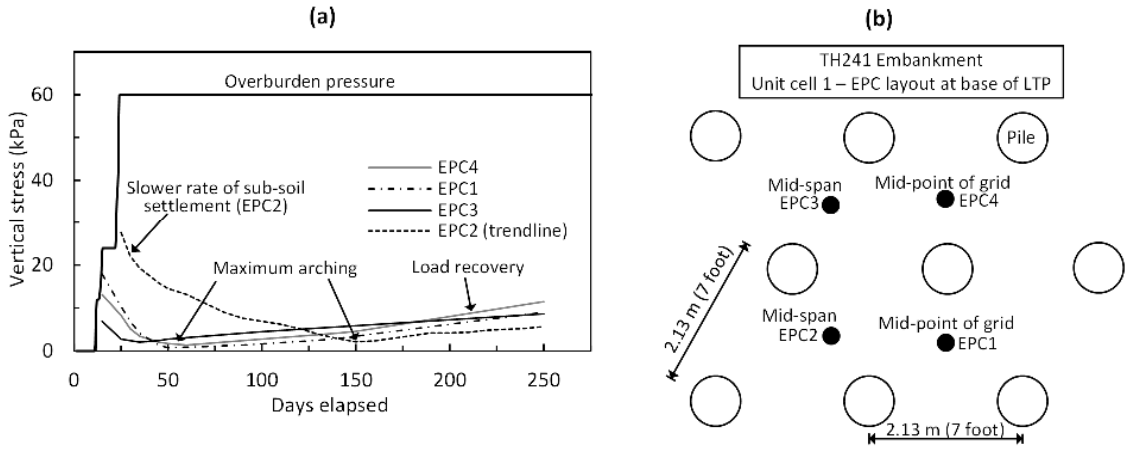

1005

1006 **Fig. 19. (a)** EPC data for TH 241 embankment and **(b)** instrumentation layout plan (modified from
1007 Wachman and Labuz 2008)

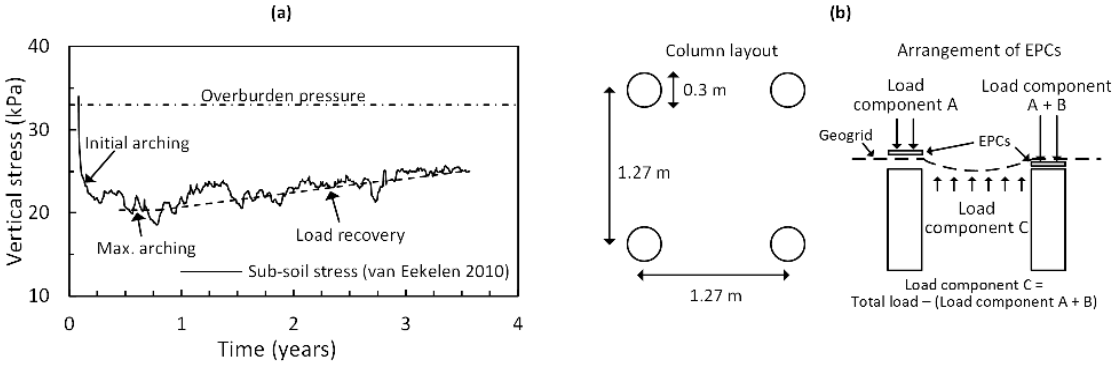

1008

1009 **Fig. 20.** Kyoto road data **(a)** Sub-soil stress (modified from van Eekelen et al 2010) and **(b)** EPC and
1010 column layout

Table 1. Properties of subsurface units

Typical thickness (m)	Geological name	Soil description	LL (%) Range (Ave.)	PI (%) Range (Ave.)	w (%) Range (Ave.)	γ_{bulk} (γ_{dry}) (kN/m^3)
2	Fill	Gravelly CLAY with some cobbles Stiff – Very stiff	-	-	-	-
7 to 14	Coode Island Silt	Silty CLAY, dark grey with marine shells Soft to Firm	34-88 (66)	11-56 (41)	31 – 75 (58)	15.6 (9.9)
3 to 6	Fishermens Bend Silt	Silty CLAY, yellow-grey, in parts sandy clay and sand Stiff to Very stiff	37	22	19	21.0 (17.0)

Table 2. ACEGrid® GG200 uniaxial polyester geogrid – manufacturer material properties

Mean ultimate tensile strength (kN/m)*	Characteristic ultimate tensile strength (kN/m) †	Geogrid characteristic strength at 2 % strain (kN/m)
219	206	52

*From results of wide-width tensile tests (ISO 10319), tested in machine direction and reported in manufacturer's literature. Cross direction strength is 30 kN/m and strain at short term ultimate strength is 10 %.
† Characteristic strength is the statistical 95 % (2 standard deviations) confidence limit.

Table 3. Timeline of embankment construction

Date	Days Elapsed	Activity
14 - 17 Jan. 2013		Detailed site investigation – CPT28 to CPT31 and BH41
March - April		Stage 1 ground improvement works (lower LTP)
28 April - 7 May		Area #2 – installation of instrumentation
3 May 8:00am	0	First manual instrumentation reading
26 - 29 June	54 - 57	Stage 2 ground improvement works (lower LTP)
5 - 13 July	63 - 71	Stage 3a ground improvement works (upper LTP)
9 - 16 July	67 - 74	Area #1 – installation of instrumentation
7 Aug.	96	Automated data logger installed
11 - 17 Sept.	131 - 137	Stage 3b ground improvement works (upper LTP)
1 Oct. - 24 Oct.	151 - 174	Embankment lifts 3 to 7
24. Oct.	174	Embankment construction complete

Table 4. Coode Island Silt consolidation parameters adopted for settlement analysis

Thickness of Coode Island Silt (m)	σ'_p (kPa)*	e_0	$C_{c\,max}$	C_r	C_α	c_v (m^2/year)	H (m)
1.7 (upper)	64 kPa (R.L. 0 m) + 20 kPa/m depth	1.0	0.4	0.03	0.002	2.0†	2.3‡
7.3 (mid)		1.5	1.5	0.11	0.006		
2.6 (lower)		1.0	0.4	0.03	0.002		

* Correlated from CPT30 q_c using expression by Lunne *et al.* (1997) and k = 0.3
† Based on laboratory testing of Coode Island Silt samples (King *et al.* 2016)
‡ H value adopted satisfies Time - U(%) relationship reported by Srithar (2010)